Revista Brasileira de Física, Vol. 2, N.° 1, 1972

Structure in the Continuum — a New Field in Heavy Ion Physics*

D. ALLAN BROMLEY
A. W. Wright Nuclear Structure Laboratory, Yale University, New Haven, Connecticut

I. Introduction

Heavy ion physics has truly come of age during the past few years. From a rather specialized subfield of nuclear physics it has grown rapidly to an overlap with almost every aspect of modem studies of nuclear structure and nuclear dynamics. Not only do the new heavy ion studies permit extension of older studies to new ranges of parameters — such as angular and linear momentum — but also they open up entirely new areas which are not accessible otherwise. These new windows into the nuclear domain have already permitted a glimpse of entirely new species — new landscapes on the uplands surrounding the valley of nuclear stability; they have also shown totally new phenomena as we move to higher altitudes in the valley itself — that is — as we move to ever higher excitation energies in our old familiar nuclear species, stable and otherwise.

It is this latter class of phenomena wich I have selected for discussion here. There are two reasons for this. First, these phenomena would never have been discovered had not a new generation of large electrostatic accelerators become available in nuclear physics. From their very beginning, Raymond Herb has played a vital and innovative role in the evolution and development of these machines; the facilities which we dedicate in this Symposium are a tribute to his inventive genius as well as to the farsighted vision of Brazilian scientists and their supporters who have moved forward in pioneering fashion to exploit these new developments. I am sure that São Paulo will soon come to play an important role in the exploration of this new terrain.

Second, these phenomena are ones which my colleagues and I have been studying as part of the research program in the Wright Laboratory at

*Work supported in part by the U. S. Atomic Energy Commission under Contract AT(30-1) 3223.

Yale in recent years. I believe that they illustrate some of the new phenomena and in particular highlight the importance of the characteristic quality and energy variability of an electrostatic accelerator beam in their study.

For several decades, in nuclear physics attention has been largely focussed on the ground and low lying levels in the nuclear species under study. In part this simply reflected the fact that the spacing of these levels was characteristically much greater than their widths and as such only reasonable resolution demands were placed on the experimental facilities; in part too it reflected the belief that until we had achieved some reasonable understanding of these lower levels, we had little hope of unravelling the higher excitation phenomena, the structure, if any, of the continuum. In fact, fundamental to our general views of the continuum, was the assumption that with so many degrees of freedom accessible to us at these higher excitations we would expect a chaotic situation amenable to broad statistical arguments. And indeed the continuum theory of nuclear interactions, based on this assumption, had many successes particularly in reproducing the characteristic phenomena of slow neutron physics.

Again, a fundamental assumption was that the characteristic level widths, reflecting the many open decay channels far exceeded the level spacings at higher excitations so that no significant sharp energy dependence of the total cross sections was expected wrresponding to high compound system energies. Ericson and many subsequent authors did show that fluctuation phenomena could result in significant structure in differential excitation functions measured at any given angle but this structure had characteristics quite different from the sharp resonance behaviour characteristic of lower system energies.

Even in the slow neutron work, however, it was found that certain simplicities remained observable even at high energies. The well known neutron strength functions were shown to be a reflection of the dissolving of a simple single-particle wavefunction describing the motion of a single neutron in the potential well represented by the target into the very large number of much more complicated continuum states in the same energy range. Then too, the giant dipole resonance in photonuclear work was shown to be a case where the underlying simple structure was described primarily by one particle-one hole wavefunctions again dissolved into those of the continuum.

More recently, the isobaric analog states have appeared as examples of relatively simple wnfigurations appearing at high excitations – in the continuum – in nuclear spectra. In this case the fact that the isobaric analog

states are of different isospin from the underlying continuum states inhibits the dissolution of the earlier examples and the analog states remain quite sharp. In light nuclei such as N^{13} for example we have found that the lowest analog state appears at something over 14 MeV of excitation yet has a width of about 2 kev. It would be completely unobservable without the higher resolution characteristic of the electrostatic accelerators. In a later paper at this Symposium I shall return to this question in discussing our studies of structure in the lead region where we have used the analog states extensively to probe nuclear structure.

What we are seeing then is unexpected structure in the continuum which we have been able to identify as the residual signature of a simple nuclear motion or configuration which has not entirely dissolved in the continuum. It is to further examples of this kind of phenomena which are suggested by our recent studies with heavy ion beams that I would now turn.

In nuclear studies with light projectiles, angular distribution measurements have played a central role. This followed because at the energies involved the number of partial waves involved was characteristically small and when a single partial wave dominated the interaction, as was frequently the case – both in direct and in compound reactions – the angular distributions provided a characteristic signature. The energy definition of the beam used was frequently of secondary importance as was the exact energy at which the measurements were to be made.

If we take a very crude estimate of the largest important orbital angular momentum in an interaction as that corresponding to a grazing collision then

$$L_{max} \sim \hbar^{-1}(A_T^{1/3} + A_P^{1/3})(2A_P E_p)^{1/2},$$

where the subscripts T and P refer to the target and projectile respectively. Clearly, for fixed E_p, $L_{max} \sim A_P^{5/6}$ and heavy ion interactions are characterized by much higher orbital angular momenta than are those induced by the more usual light ions. This, of course, can be a unique advantage in providing access to high spin states as I shall illustrate below; it carries with it, however, the disadvantage that as more and higher partial waves contribute the direct angular distributíons carry less unambiguous information and the excitation function – the variation of cross sections with energy rather than angle – takes on much increased importance. For this the ready energy variability of the electrostatic accelerator is of central importance. As I shall illustrate below we have found, indeed, that only by obtaining extensive simultaneous data on both energy and angle varia-

tions of cross section and fitting them simultaneously are we able to provide stringent tests for model and mechanism hypotheses.

Although they represent only a part of our current heavy ion research activity I have chosen to focus on three general areas to illustrate my general thesis concerning new phenomena in the continuum. As the simplest possible interaction, and one whose understanding underlies all that of more complex phenomena I turn first to elastic scattering; even here we have seen such phenomena. Next I shall consider the simplest possible direct reaction, the transfer of a neutron, but will examine this in a new way only possible in heavy ion physics where the neutron wavefunction at very large radii can be probed. Finally, I shall consider the question of recently discovered very sharp, high spin states in the continuum – using Mg^{24} as the example – which our recent measurements suggest may have quasi-molecular structures wherein one or more alpha clusters, or more generally, quartets, may play an important role.

In the course of this discussion I shall have occasion to draw attention to the essential role played by high beam quality and energy variation; no less important has been the use of a relatively complex computer based data acquisition system. Particularly in the study of continuum states with many open decay channels it becomes of extreme importance to *overdetermine* the experimental parameter situation in order to avoid ambiguities and uncertainties of interpretation and in order to extract data on relatively weak decay channels in the presence of much more prolific ones. The characteristics of heavy ion reactions significantly exacerbate all these intrinsic difficulties.

2. Elastic Scattering Interactions

The study of the energy dependence of the elastic cross section offers one of the most complete and reliable possibilities for the determination of the heavy ion interaction potential.

In our studies of the elastic channel we have chosen to concentrate initially on the interaction of identical boson systems; the symmetries thus introduced, as we shall show below, greatly simplify the analysis and permit greater insight into the scattering phenomena involved. We shall include here appropriate data on scattering of nonidentical systems both from our own laboratory and from others. We shall present herein a rather detailed study of the physical phenomena which underly the description

of the scattering on an optical model basis. This, in particular, will focus on the gross structure in the experimental excitation function data which we shall attribute to scattering states in the continuum. Overlying this structure but yet intermediate in widths between it and the more usual statistical fluctuations we have found structure which Greiner et *al.*[1] have succeeded in reproducing qualitatively on the basis of a double resonance phenomenon also involving scattering states in the continuum.

In recent years, a considerable number of interesting, often surprising, data have been collected using EN, FN, and MP tandem accelerators[2-9]. Usually, severa1 elastic scattering excitation functions have been measured at different angles. Indeed, we have found that fits or analyses of isolated angular distributions or to a lesser extent single angle excitation functions can frequently be worse than meaningless because fluctuations at any given energy can lead to quite erroneous conclusions conceming the interaction potentials involved. In order to compare the results for identical and for non-identical systems on a common basis, however, we shall consider only the 90" scattering situations.

Figure 1 shows that all the presently available data on excitation functions present a similar gross structure, typically a few MeV in width. The $C^{12} + C^{12}$ data have been energy averaged to emphasize their gross structure aspects.[10] It should be noted that this characteristic width decreases systematically in going to heavier systems. We return to this point below. Only the nonidentical $O^{16} + N^{14}$ and $O^{16} + N^{15}$ systems appear as exceptions. The $O^{16} + O^{16}$ and, especially the $C^{12} + C^{12}$, scattering data also present well defined intermediate structure of narrower width (0.3 to 1.2 MeV), while as usual a very fine structure bewmes evident as the system energy resolution is increased to $\sim$ 10-20 keV[5]. Figure 2 shows this intermediate structure more clearly.

In recent years many studies, all based on optical model calculations, have been devoted to the interpretation of the gross structure and in particular that observed in the $O^{16} + O^{16}$ system[3,5,11-14]. The dashed curves of Figure 1 are the optical model predictions obtained in calculations based on the Woods-Saxon optical model parameters determined by Maher et *al.*[5] in their original study of the $O^{16} + O^{16}$ scattering. Only the interactian radius was scaled as ($A^{1/3}$) in adapting the $O^{16} + O^{16}$ parameters to the different systems in these calculations. The predictions do produce a correct width for the gross structure, although the exact positions of maxima and minima as well as the relative magnitudes, as expected, require more precise matching by residual parameter variation from case to case. In all

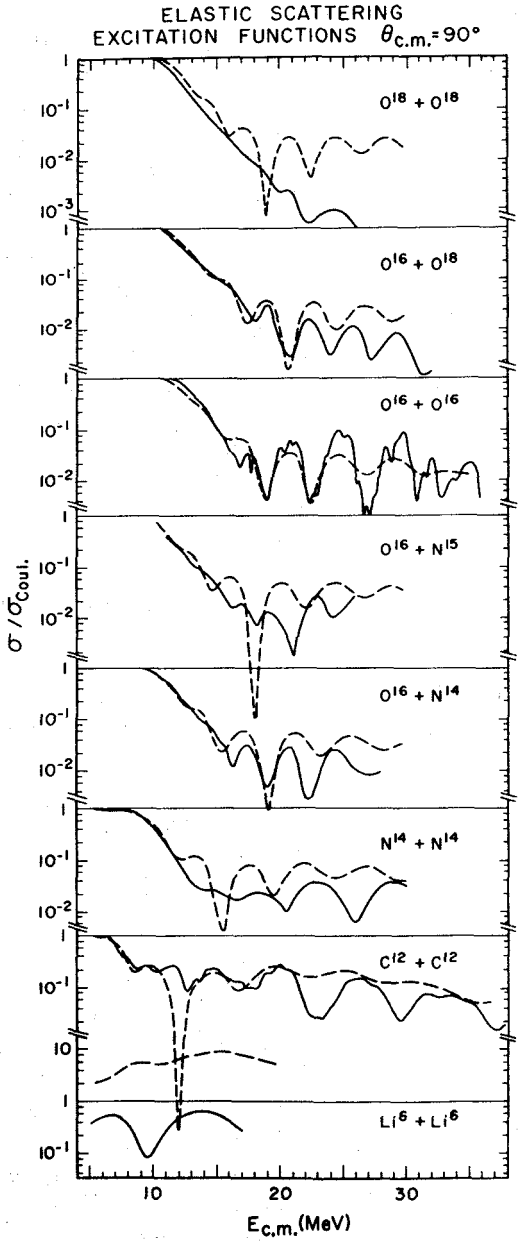

Fipre 1 - Collected heavy ion elastic scattennq excitation functions. The *full lines represent* data, while the dashed lines are optical model predictions.

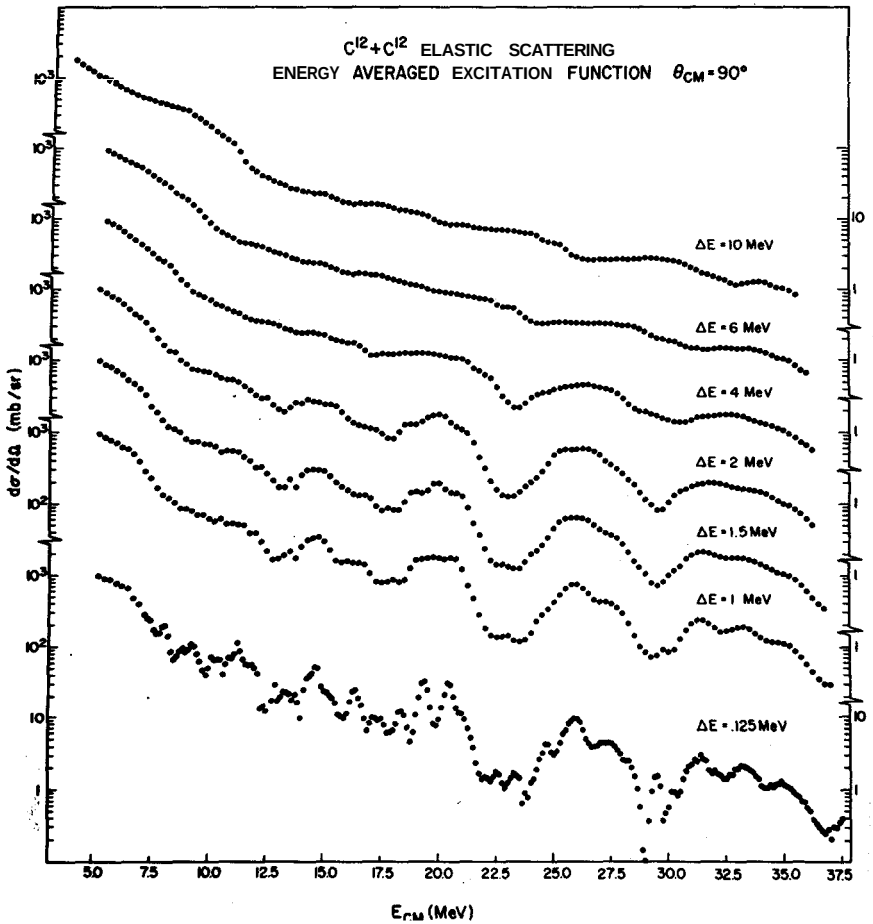

Figure 2 - Energy averaged 90" excitation functions for the $C^{12} + C^{12}$ scattering system. The energy averaging intervals are shown on the figure for each case. The structure of intermediate width appears clearly only at the $\Delta E = 0.125$ MeV level; marked fluctuation structure becomes evident at AE $\lesssim$ 0.050 MeV. The systematic increase in the apparent width of this intermediate class of structure from some 0.600 MeV to 1.20 MeV in the energy range shown here appears in excitation functions measured at other angles as well.

these extrapolated cases the predicted cross sections lie above the experimental values reflecting the strongly bound character of O^{16}

In Figure 3 we again present the series of five excitation functions measured for the $O^{16} + O^{16}$ scattering. In part a) we include the original optical

model fit obtained by Maher *et* al.; in part b) we show the improvement obtained by Chatwin *et al.*[13] through introduction of a specific dependente of the model parameters on the orbital angular momentum involved and in part c) we demonstrate that essentially equivalent fitting can be achieved without introduction of the two additional parameters of the L dependent model through modification of the normal Woods-Saxon parameters – in particular through marked reduction of the diffuseness from 0.49 to 0.15 F as is perhaps not physically unreasonable for the doubly closed O^{16} nucleus. It should be noted, too, that in the modified potential the imaginary well has been pulled inside the real well; this situation favors orbiting and possible resonating of the higher partial waves over that used in the original analyses.

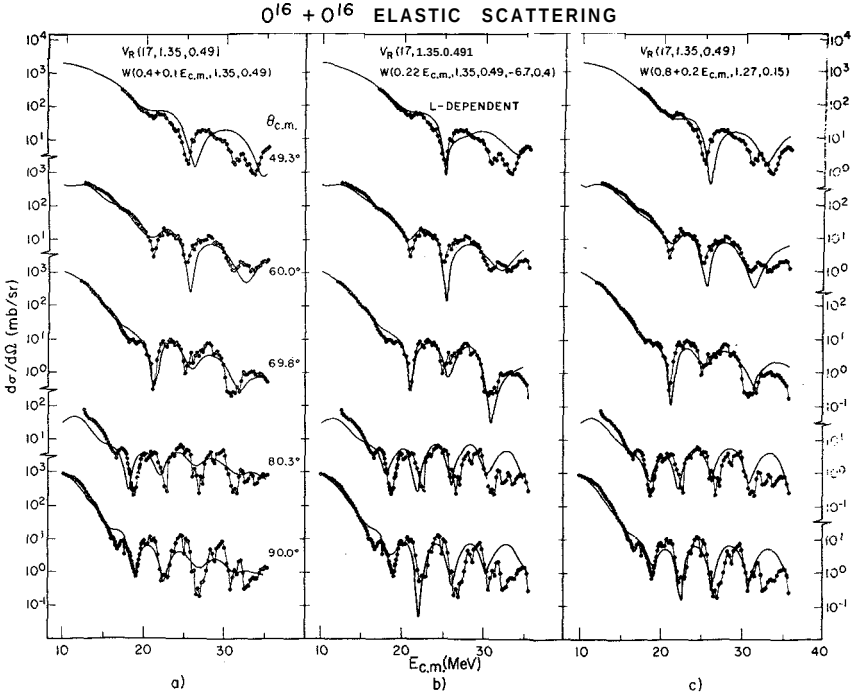

Figure 3 - Optical model fits to the $O^{16} + O^{16}$ **data.**

On the basis of such a demonstration we have chosen to focus our attenticn on the simple optical model, without any of the suggested modifications,

in an attempt to better understand the detailed nature of the scattering interaction within the simplest possible model framework.

Figure 4 is a schematic representation of the $O^{16} + O^{16}$ scattering situation. At the extreme left are shown the real potentials for the different partial waves and for the model parameters appropriate to Figure 2c). Next are shown the real phase shifts 8, and the reflection coefficients $A_{,}$, the 90° differential excitation function and finally an energy-angle surface of the calculated elastic scattering wrresponding to these model parameters, plotted at 0.25 MeV energy intervals.

Several observations are important here. At low energies – and L values – the scattering is characteristic of an absorptive potential in that the corresponding radial wavefunction, being able to penetrate deeply in the nuclear interior, is subject to strong absorption. The corresponding phase shifts δ_l are negative. With increasing energy and L values – the internal reflection barrier moves to larger radius where it affects the radial wavefunctions more strongly and the phase shifts go positive. It should also be noted that as each phase shift departs from zero the corresponding reflection coefficients A, changes quite rapidly from 1 to 0. Each partial wave is thus active over only a relatively restricted range of energy. This situation is particularly marked in the case of identical particle scattering, as here, since the total absence of the intermediate odd orbital angular momenta implies that at a given energy, at least above some 15 MeV, the scattering is dominated by a single partial wave. This is strikingly evident in the similarity of the calculated angular distribution at the indicated energies to a simple $|P_L(\cos\theta)|^2$ form; this is clearly borne out in the experimental data In Figure 4, it is possible to follow the systematic evolution of this behavior. As indicated, the maxima M_0, M, , M_2, etc. in the 90° differential cross section at $E_{CM} \cong 21, 25, 29$, etc. MeV are attained at the same energy as the $|P_L(\cos 8)|^2$ angular distribution. As an example, for L = 18, $A_{L=18}$ begins to deviate significantly from 1 at about M, and the complete absorption situation for this partial wave is reached at M_2 ; in the interval a deep minimum, m_1, at E_{CM} r 27 MeV is generated in the 90" differential cross section when $A_{L=18} \cong .5$. A $|P_{L=18}(\cos 8)|^2$ angular distribution begins to emerge at E = 27 MeV, reaches its clearest definition at $E_{CM} = 29$ MeV and disappears to be replaced in turn by the L = 20 phenomena.

Inspection of the experimental data on $O^{16} + O^{16}$ in Ref. 8 shows that ar the highest energies studied, E_{CM} r 40 MeV, the gross structure in the 90" excitation function was effectively damped out; reference to Figure 4

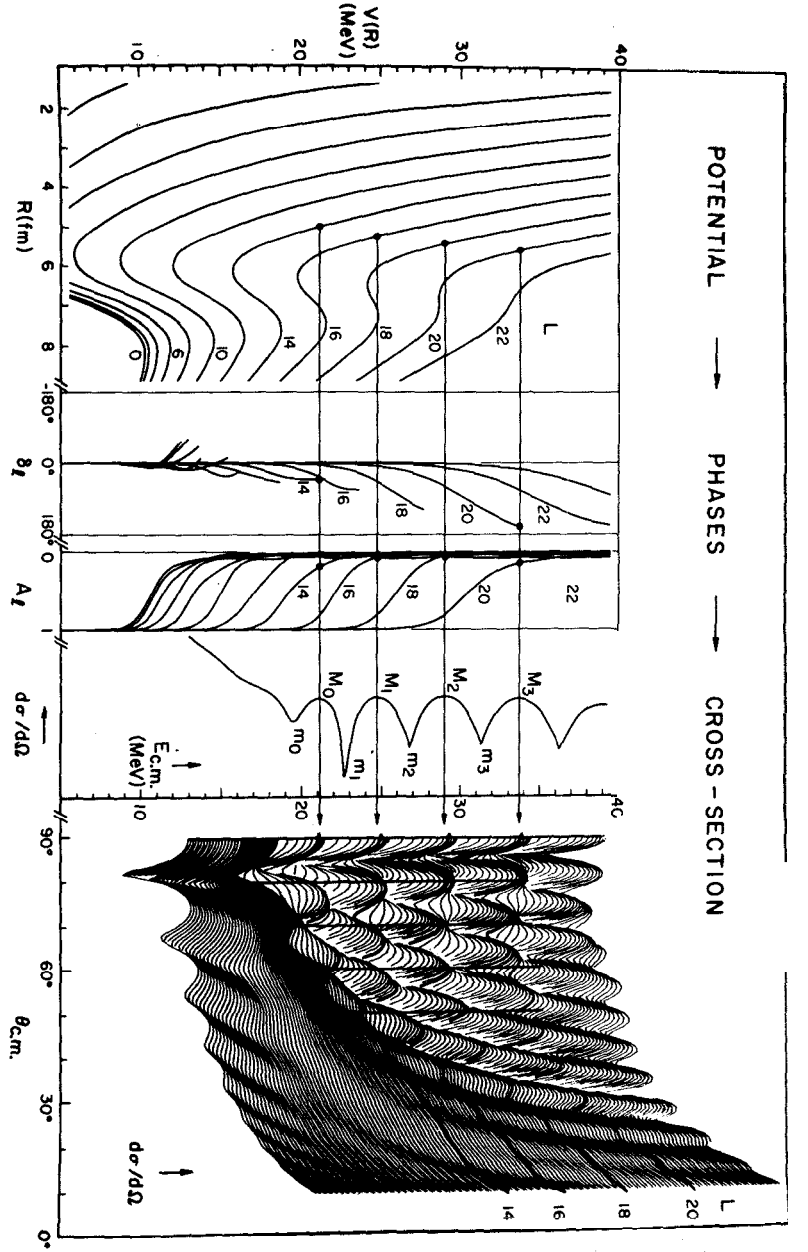

Figure 4 - Optical model representations of the $O^{16} + O^{16}$ elastic scattering.

shows that such behavior provides strong support for the physical reality of the abnormally shallow real potentials which we have used consistently in our work in this mass region. With a much deeper real well as would be suggested by the discrete ambiguity prescription, for example, the gross structure would be predicted to persist to much higher energies than is observed.

It should be noted in passing that the surface presentations such as that on the right of Figure 4 are readily available with even modest computational facilities and are of considerable utility in visualizing overall characteristics of a complex body of data. This is already apparent in Figure 4 where the vertical heavy lines mark the angles at which the original excitation function data were obtained; from this presentation it is already obvious that at certain energies there is pronounced sensitivity of cross section to small angular changes which readily explain the earlier somewhat puzzling experimental difficulties which were encountered in obtaining consistent experimental data in repeated studies of these regions. The striking transition from Mott scattering to nuclear scattering with increasing energy is also very apparent in this presentation.

In Figure 5 we illustrate again this utility in confronting the model calculations with detailed experimental data measured at narrow energy intervals in the range $19 \leq E_{} \leq 22.25$ MeV. The gradual evolution of the additional maximum characteristics of higher P_L^2 is well reproduced.

Going from an identical to a nonidentical system the predicted energy angle surface looks, at first sight, completely different as shown in Figure 6. As we have already shown, however, the excitation function for $\theta_{CM} = 90°$ has precisely the same shape in both cases. Identical optical model parameters have been used in both cases. It is interesting to note that for nonidentical particles the structure of the excitation functions for $\theta_{CM} \sim 180°$ is very similar to the structure at $\theta_{CM} \sim 90°$ in the case of identical particles. In the former, however, the number of expected maxima is doubled because not only even but also odd partial waves contribute to the scattering. We have initially focussed attention on the identical particle systems for several reasons: the interesting structure at $\theta_{CM} \sim 90°$ can be studied where the cross section is large. Only even partial waves contribute to the scattering so that the influence of a single partial wave can be more readily isolated and investigated over a wide energy interval. Compound elastic contributions ar $\theta_{CM} = 90°$ are also expected to be relatively small compared to the possible contributions at 180° and finally contributions from exchange processes are possible in these cases only in second order. We shall

return below to our later measurements and analyses of nonidentical systems where these exchange terms can play important and often dominant roles.

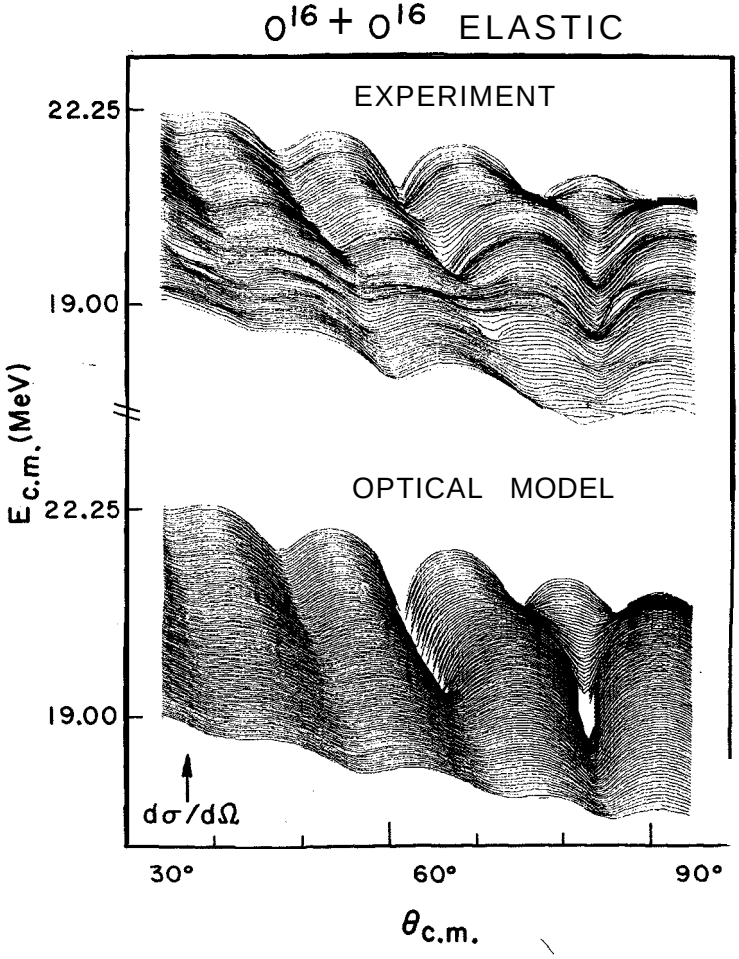

Figure 5 - Optical model calculations compared with interpolated $O^{16} + O^{16}$ data.

3. Phase Shift Behavior

Returning to the identical particle case it is possible to obtain a fuller understanding of the behavior of individual partial waves in the scatte-

ring through construction of the familiar Argand diagrams shown in Figure 7. Here the behavior of the L = *16, 18,* and *20* partial waves, as shown in Figure 3, is examined in detail. In parts a), b), and c) the function $A_l e^{2i\delta_l}$ is displayed, whereas, in parts d), e), and f) the function $1-A_l e^{2i\delta_l}$ is displayed through simple translation of the origins to $X_l = 1$ and $Y_l = 0$. These latter three partial wave amplitude plots display very similar features.

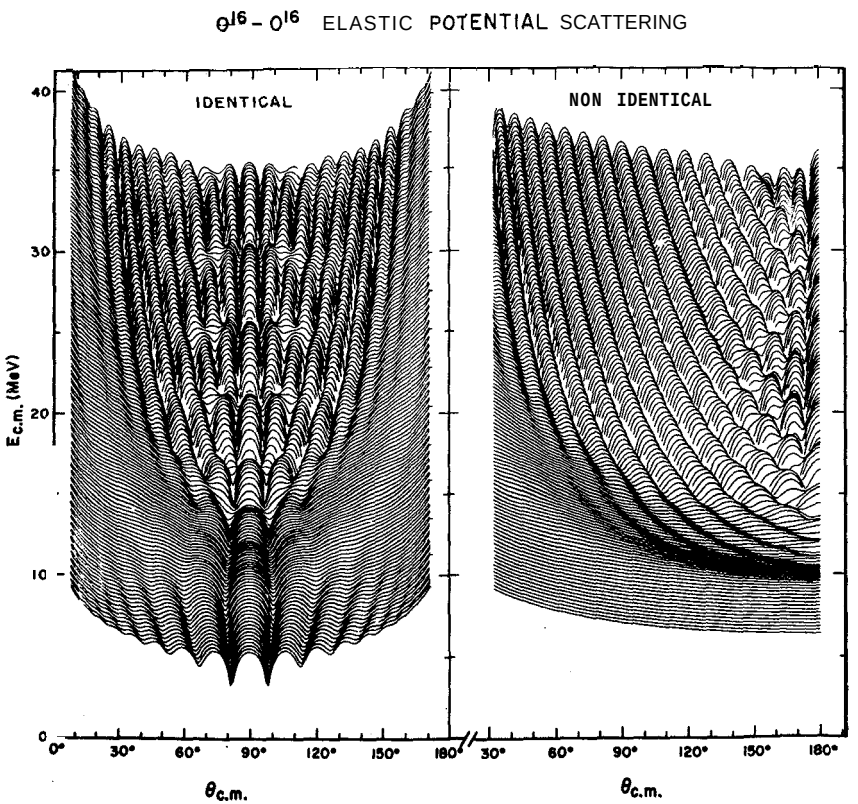

Figure 6 - Optical model calculations with and without symmetrization.

At the energy where a given partial wave begins to contribute significantly to the cross section a fast rise in the partial amplitude and almost no change in phase is observed. With increasing energy a region occurs wherein the partial amplitude is stationary because the Coulomb and nuclear phase shifts move in opposite directions.

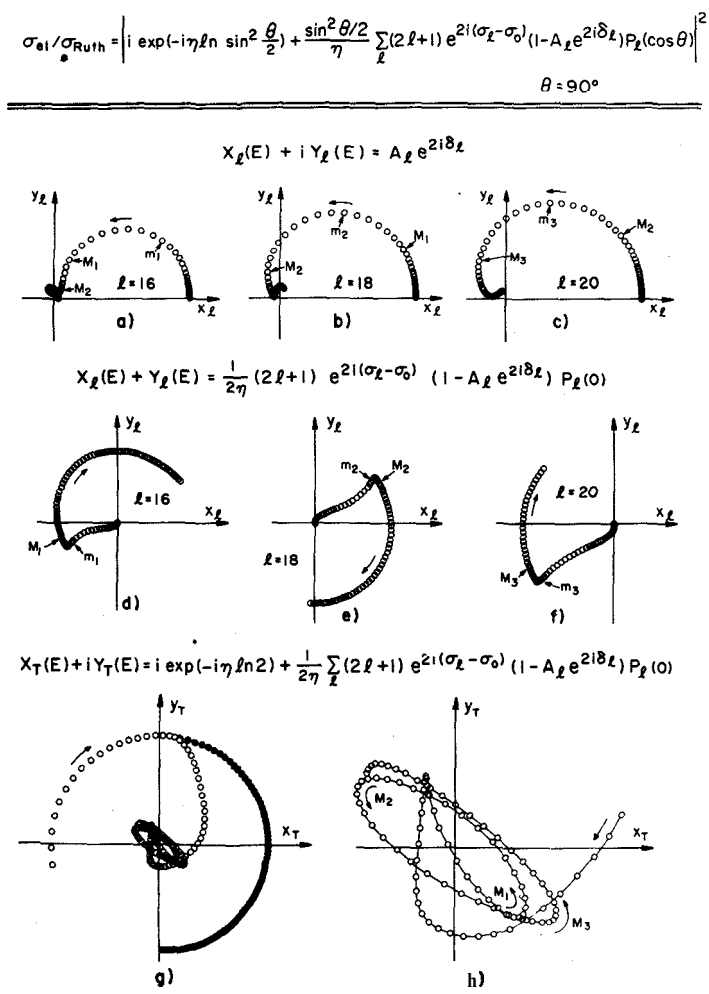

Figure 7 - Vector diagrams for identical particle elastic scattering.

To illustrate how the 90" **excitation** function is generated in the energy interval $\mathbf{20 \leq E_{CM} \leq 34\ MeV}$ we **consider** the L = **20 partial** wave. This **first deviates** from zero at E_{CM} **r** 20 **MeV** where **all** the lower L amplitudes are essentially vectors of **constant** length **moving** with **the** Coulomb phase; these amplitudes add coherently with the **first term** of unit length to form a smoothly varying background (Coulomb phase shifts vary smoothly with energy). The magnitude of the L = 20 partia1 waves **in-**

creases rapidly with energy interfering destructively with the background After the minimum m_3 is reached the L = 20 amplitude remains essentially constant but the background phase varies so that the cross section again increases.

The last two diagrams (Figures 7g and 7h) display the total scattering amplitude. At low energies the Coulomb term dominates. However, at higher energies the interference of different partial waves reduces the cross section. The origin of the oscillations in the 90° differential cross section are particularly evident in Figure 7h which is an enlargement of the central region of 7g.

For a better understanding of the mechanism generating the shape displayed by the Argand diagrams a), b) and c) of Figure 7, we have systematically decreased the magnitude of the imaginary part of the complex potential in order to magnify the shape effects caused by the real potential. The results obtained for the L = 18 partial wave are given in Figure 8: c = 1 represents the starting situation of Figure 7b; for c = C the absorptive imaginary part has been completely eliminated; as expected the real phase moves, as a function of the energy, along the unitary radius. It is interesting

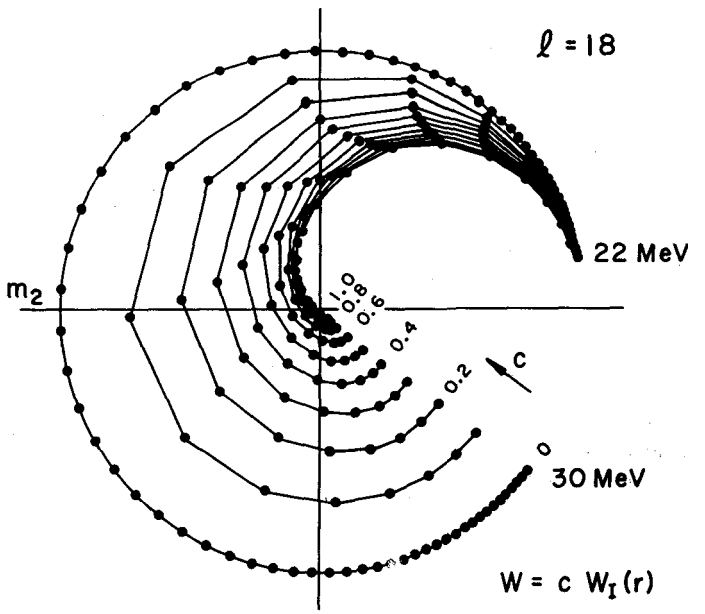

Figure 8 - Argand diagrarn displaying the energy dependence of the scattering function for l = 18 for an imaginary potential of variable magnitude.

to note that for c = 0 an almost perfect resonance like behavíor is observed, with a slow change of the phase at the extreme energies and a much more rapid change in the region of $\delta = 90°$. This energy corresponds to the minima m_2 of Figure 4, where the L = 18 partial wave is affected by a rapid change in the shape of the corresponding potential barrier. The effect of the increasing imaginary potential in masking this classic resonance behavior is obvious in Figure 8.

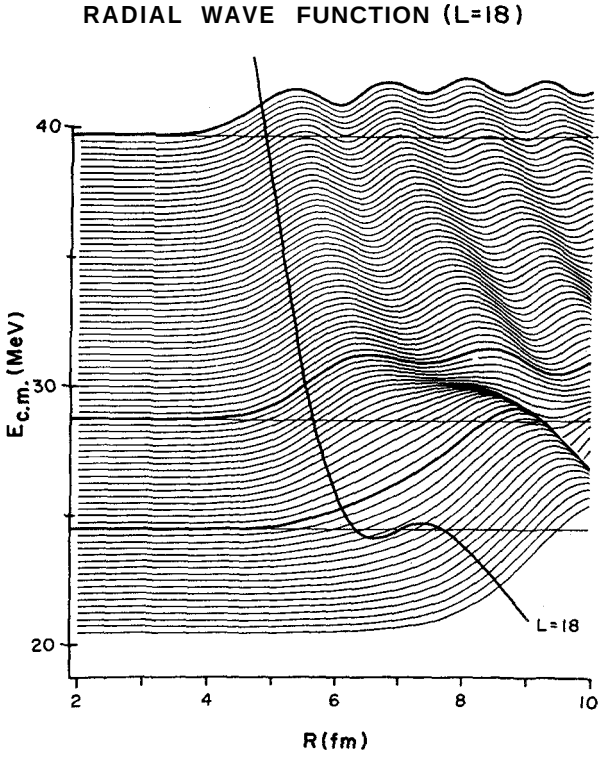

Figure 9 - Amplitude of the L = 18 radial wave function in the $O^{16} + O^{16}$ scattering as a function of radius and center of mass scattering energy. The heavy solid line is the real optical model potential appropriate to L = 18.

Figure 9 displays the radial dependence of the L = 18 partial wave as a function of the bombarding energy. For any given energy, the modulus of the amplitude obtained from the integration of the wave equation in the complex well is plotted as function of the radius. What is represented,

therefore, is the sum of ingoing plus outgoing flux. Above 30 MeV the partial wave is absorbed (see Figure 4) consequently the amplitude shown here corresponds essentially to the ingoing flux. Below 20 MeV what is observed is a complete reflection by the Coulomb barrier. At an energy where nuclear interaction first occurs, the incident wave is attracted inside the potèntial well, its magnitude remaining quite large. This is the most critical region of the heavy ion interaction, and as evident here it is dominated by a surface mechanism where the collision time is relatively long and possible orbiting can occur. It should be noted that this orbiting condition has much in common with a metastable quasimolecular state; a transition from the orbiting condition to a more strongly bound quasimolecular state, as is implied in a number of the mechanisms which have been suggested to explain the intermediate structure in the scattering data, is thus a natural one.

An extension of this picture follows in analogy with the familiar DWBA calculations where overlapping of wavefunctions of different reaction channels is invoked It is clear that a large amplitude for one single partial wave at energies just above the attractive part of the potential will favor situations with flux going to surface phenomena such as inelastic scattering or transfer reactions (good overlap between wavefunctions). Equivalently elastic scattering receives strong contributions from the surface effects if the matching conditions of energy and angular momentum are favorable. For a more detailed description of matching conditions see Ref. 1, 15, 16.

It follows from all of this that within the framework of an optical model it is possible to identify specific energy and angular behavior of the elastic channels with particular partial waves; however, the classical resonance behavior is masked by the absorption presented as we have discussed above. In particular we are able to reproduce the gross features of both the energy and angle dependence of the scattering cross sections in terms of relatively simple resonant situations involving an orbiting of the incident particle in the optical well. Before proceeding to the structure of intermedíate width, whose structure may involve a double resonance phenomenon based on these orbiting states, it may be useful to quote the actual optical model parameters which we have found to reproduce our data.

4. Optical Model Parameters

We have already shown that scaling of the $O^{16} + O^{16}$ potential parameters of Figure 2 to the remaining systems provides a useful representation of

the experimental data and a base for analyses of more complex interactions. As a matter of record we include in Table I herewith the parameters which we have found to provide the most realistic fits to the $O^{16} + O^{16}$, $N^{14} + N^{14}$ and $C^{12} + C^{12}$ data when a more extensive parameter search was invoked. (In the latter two cases the searches have been restricted to equal real and imaginary radii and diffuseness.)

SYSTEM	V(MeV)	r(F)	a(F)	W(MeV)	r_I(F)	r_o(F)	a_I(F)
$O^{16} + O^{16}$	17.0	6.80	0.49	$0.4 + 0.1 E$,	6.80	1.35	0.49
	17.0	6.80	0.49	$0.8 + 0.2 E_{CM}$	6.40	1.27	0.15
$N^{14} + N^{14}$	15.0	6.50	0.49	$0.4 + 0.125 E_{CM}$	6.50	1.35	0.49
$C^{12} + C^{12}$	14.0	6.18	0.35	$0.4 + 0.1 E$,	6.41	1.40	0.35

Table I - Extracted optical model parameters. In the latter two cases, the searches have been restricted to cases of equal real and imaginary radii and diffuseness.

The first entry in Table I is the original $O^{16} + O^{16}$ potential evolved by Maher et *al.*[5]; the second is that corresponding to Figure 2c). The systematic decrease in a, in going from N^{14} to O^{16} may well be physically significant in moving from a loosely to a very tightly bound system.

Of particular significance here is the shallow potential which we find best suited to reproduction of the experimental data. There have been a number of reported theoretical attempts to derive such a shallow interaction potential from more fundamental considerations. These were discussed in some detail in a recent review[10] and will not be considered in any further detail here. It is of interest however to wmment on the results of a schematic model developed by Scheid, Ligenza and Greiner[11] which uses as its fitting parameter the compressibility of the O^{16} nuclear matter. The value for the compressibility which emerges from these studies is 200 MeV which is smaller by a factor of three than has frequently been quoted for this parameter. Recently however Bethe[17] has shown that a compressibility of this magnitude is essential to the model of finite nuclei which he and his collaborators have developed from fundamental nuclear matter considerations. It will be of very considerable interest to extend the Scheid et *al.*[11] analyses to other systems to search for any systematic variation in the wmpressibility with nuclear structure.

5. Coupled Channel Analyses

It is clear that particularly in those systems where the interacting ions have low excited states with strong collective coupling to the ground state, or where non-elastic mechanisms such as transfer can proceed with large amplitude, the representation of all non-elastic processes through a simple imaginary potential cannot be expected to be adequate and a coupled channel treatment which explicitly treats the dominant non-elastic amplitudes becomes mandatory[18-20]. A number of rather schematic models have been evolved to treat explicitly certain selected classes of non-elastic processes; we shall mention one of these briefly before retuming to the more complete coupled channel approaches.

Although the range of masses thus far studied experimentally, as indicated in Figure 1 for example, is relatively restricted it does span a marked difference in overall collectivity, as between C^{12} and N^{14} for example. It might be expected, therefore, that explicit consideration of the strong collective inelastic channels might be essential in achieving a more satisfactory representation of this range of data

It may well be that some of the structure which appears in the experimental data may reflect mechanisms wherein the strongly collective states function as doorways through which much more complex compound nucleus configurations are coupled to the elastic channel. It seems important, however, before attempting to treat this complicated mechanism in any detail to focus first on the direct coupling of the collective states themselves to the elastic channel.

An interesting mechanism involving double resonance and coupling between elastic and inelastic channels has recently been proposed by Scheid, Greiner and Lemmer[1] in order to explain the intermediate structure observed in the $C^{12} + C^{12}$ and $O^{16} + O^{16}$ scattering data. Although their description of the resonances disagrees in some aspect with our observations (the energies at which they were located were the maxima and not the minima of the 90° excitation function, and different L values were assigned to the individual resonances) the characteristics of the orbiting resonance described herein correspond very well with the specification of their socalled "virtual state".

In this model, which is reminiscent of that evolved by Imanishi[21] in an attempt to reproduce the original $C^{12} + C^{12}$ quasimolecular states observed by Bromley et *al.*[22], Scheid et al. propose that during the effective

"resonant" interaction orbiting of the ions provida an opportunity for temporary inelastic excitation of one (or both) of the scattering nuclei with corresponding temporary decrease in the available kinetic energy. If this decrease is such as to reduce the incident kínetic energy to that of a quasi-bound state in the effective real potential the condition for a double resonance occurs and the intermediate structure is assumed to reflect the different possible couplings of the angular momentum of the original orbiting "resonance" and that of the quasibound state.

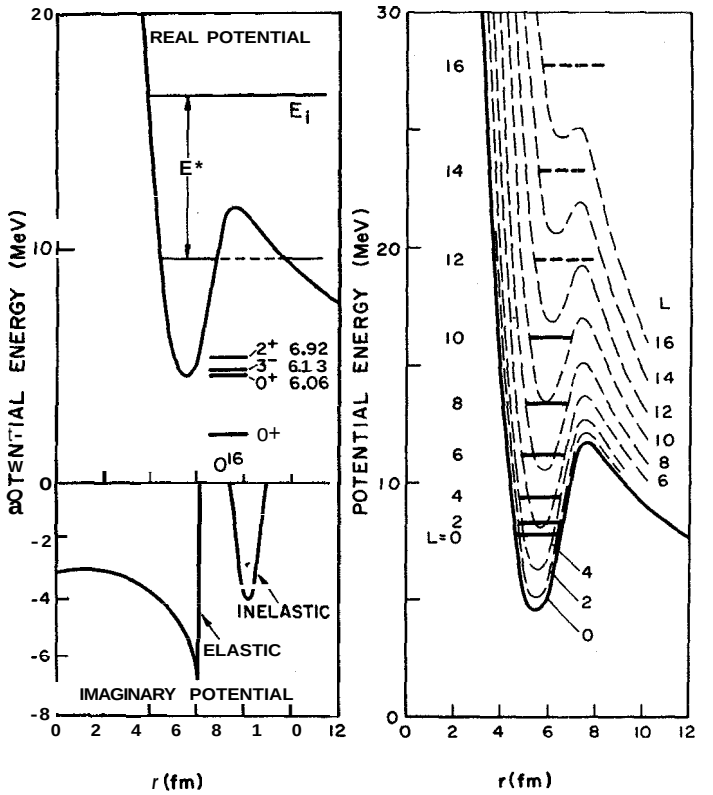

Figure 10 - Model potentials calculated by Scheid, Greider and Lemmer for the $O^{16} + O^{16}$ case. The real potentials for different partial waves are shown on the rigth and the corresponding imaginary potentials on the lower left. The upper left figures is a schematic illustration of the double resonance mechanism discussed in the text.

Figure 10 illustrates this model and is taken from the work of Scheid et *al.*[1] as is Figure 11 which presents the results thus far obtained in the $O^{16} + O^{16}$ case. On the right are shown the potentials appropriate to different partial waves in the scattering interaction. The real nuclear potential in this instance was derived from a Thomas-Fermi model calculation but its features are quite similar to those of the optical models discussed above. Clearly there are bound (or really quasi-bound) states in such potentials as indicated by the full lines; with increasing orbital angular momentum there occur the orbiting, or scattering, states discussed above and here shown as the dashed lines.

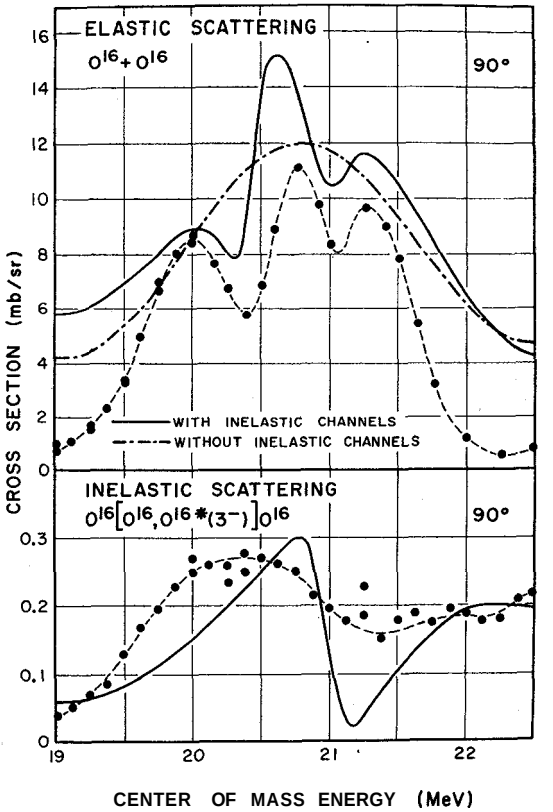

Figure 11 - Results of calculations using the model potentials of Figure 10, compared with Yale experimental data on both elastic and inelastic scattering in the $O^{16} + O^{16}$ case. Experimental data points are shown.

If, as suggested on the left of Figure 2, the energy E_i is appropriately chosen a continuum scattering resonance is observed corresponding to one of these dashed states; this leads to the gross structure observed in the elastic scattering excitation functions. If now, an excitation of one of the ions (or both) occurs with a loss of E* in kinetic energy there exists the possibility that the system will at least temporarily find itself again in a quasi-bound state. If, in particular $E_i - E^*$ happens to correspond to one of the few bound states in the potential appropriate to a lower partial wave, a double resonance situation can occur. The lower figure on the left illustrates the very crude first approximation imaginary potentials which Scheid *et al.*[1] have used in this first calculation and which they have deduced from very general considerations of the interaction characteristics.

Figure 11 shows the initial results attained in comparison to our experimental data. Clearly the model is capable of at least generating the proper type of intermediate width structure. In particular the secondary minimum at 20.3 MeV results from excitation of the 2^+ state at 6.92 MeV in O^{16} through the elasfic partial waves with L = 6, 8, and 10 which resonate with the L = 8 quasi bound state at 13.4 MeV. Correspondingly the minimum at 21.0 MeV results from excitation of the 3^- state through the L = 12 elastic partial wave and a resonance with the L = 9 quasi bound state at 14.8 MeV. The lower part of this figure is a comparison of the corresponding calculation of the direct inelastic excitation of the 3^- state with our experimental data Again reasonable qualitative and even partial quantitative agreement has been obtained. While emphasizing, as do Scheid *et al.*[1], that these calculations must be considered as very crude and preliminary the results are encouraging. In our own laboratory Professor Ascuitto is currently completing modifications in his major coupled channel code such that he can handle the necessary angular momenta etc. to permit examination of these particular situations. It will be of greatest interest to apply these techniques to the $C^{12} + C^{12}$ system where as shown in Figure 2 the intermediate width structure is very clearly marked and the inelastic scattering cross sections are known to be higher.

It is apparently the case, however, that in these heavy ion scattering interactions, the possibility of interim excitation of low levels of the projectile itself can give rise to double resonance phenomena which appear as marked structure in excitation functions, superimposed on the strong fifty to one peak to valley structure of the orbiting resonances at energies which correspond to many tens of MeV into the continua in the compound systems.

6. Experimental Techniques

It may be worthwhile mentioning briefly the type of instrumentation which we now use in such studies.

Heavy ion reaction studies are plagued, particularly at energies well above the Coulomb barriers, by the problem of very many open reaction channels. This implies not only a small cross section for each channel but also a very large background What is required is then an experimental system possessing intrinsically large data collection efficiency together with an unusually high degree of selectivity in identifying the events of interest in the high background radiation from the target.

All measurements reported herein have utilized heavy ion beams from the MP tandem accelerator in this laboratory and the IBM 360/44 computer based data acquisition system developed as a joint study between this laboratory and IBM[23,24]. The high efficiency has been attained through use of large solid angle linearly position sensitive semiconductor detectors (PSD) and the identification has been achieved based on the unique kinematic characteristic of each of the events of interest. The high data rate of our system then permits simultaneous data acquisition on all the events of interest.

Typically we have used two PSD units positioned to subtend some 20° of angular aperture at the detector and have wnnected these in a five parameter coincidence configuration for data acquisition[25]. These five parameters are the energies of the charged particles in each of the two detectors (E_3 and E_4), the position (hence angle θ_3 and θ_4) of laboratory emission of each of these particles, and the relative time interval T between their arrival at the detectors.

Shown in Figure 12 are the kinematic loci for the most important interactions in the $C^{12} + C^{12}$ and $C^{12} + C^{13}$ collisions. The indicated rectangle in the first quadrant, i.e. the angle of particle 1 (θ_3) versus the angle of particle 2 (θ_4), covers the region of observation accessible to the two PSD's at a given geometric setting. The heavy line segrnents in the remaining quadrants correspond to those regions of observation which are also selected by the coincidence conditions. Such a system possesses several advantages in wmparison to a more traditional kinematic coincidence arrangement: In the simple original arrangement the wrresponding rectangles in Figure 13 converge to poínts and only one specific, preselected reaction is detectable. This provides no opportunity of detecting any new

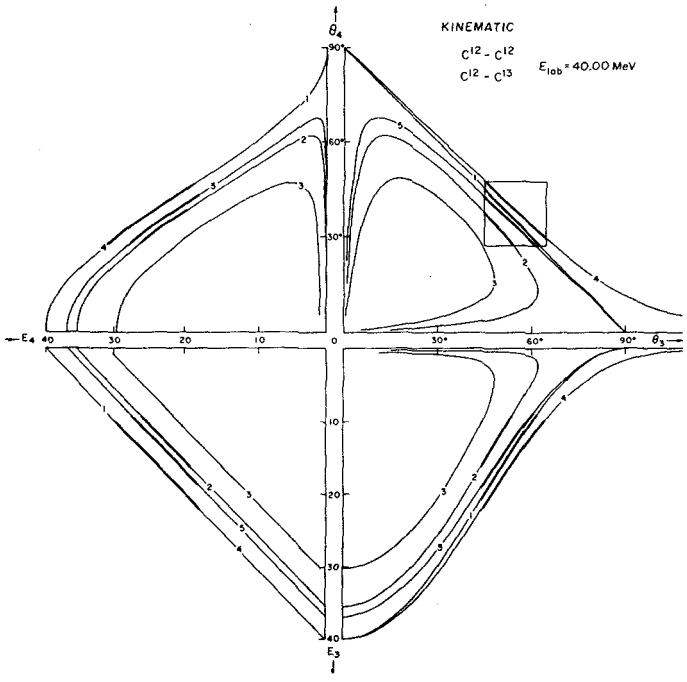

Figure 12 - The kinematic diagrarn for $C^{12} + C^{12}$ and $C^{12} + C^{13}$ interactions for an incident C^{12} energy of 40.00 MeV.

or unexpected processes if such are present. The simultaneous observation of all kinematic variables which this system permits and its available resolution enables a precise selection of the processes under consideration and an effective elimination of the unwanted background; unexpected processes are clearly included. Figure 13 illustrates schematically the logic used in processing the information furnished by both PSD's: energy and position for each of the charged reaction products (E, , P_1 , E,, P,). The Yale-IBM data acquisition system has been described elsewhere in detail[23]. The 5 analog inputs (E,, P_1 , E,, P_2 and T) are each connected to a 25 Mhz 1024 channel ADC allowing multiparameter analysis with good resolution at high rates. The event pulse shown in Figure 13 causes sampling of the 5 ADC's. The digital information is fed into a buffer area in the computer memory. When the buffer is filled the information is logged on magnetic tape and is also processed online by appropriate data acquisition analysis routines. Various transformations on the data such as the reduc-

tion of position to angle information, the identification of specific reaction channels, the automatic elimination of background and the like are all readily performed on-line. The accumulated spectra can ben monitored on-line using an interactive cathode ray tube terminal (display) with a powerful light pen facility. Of particular interest is the ability to select any given region of any one or two dimensional spectrum, i.e. set a gate, by simply drawing an arbitrary contour around the region of interest with the light pen. This is particularly advantageous in eliminating problems which would otherwise be associated with intrinsic response non-linearities of the PSD's.

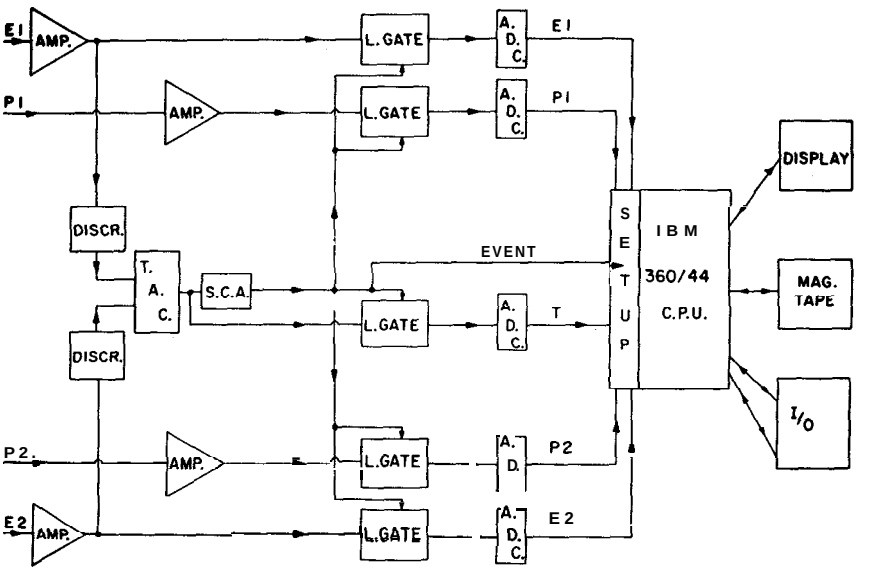

Figure 13 - Schematic diagram of the data acquisition system.

Figure 14 shows data accumulated during a $C^{12} + C^{12}$ scattering experiment. Kinematic lines similar to those of Figure 12 can be recognized in Figure 14a), b), c), and d). The analyses are based on the possibility of replaying all the data logged on the tape after the setting of appropriate gates. Such a gate photographed directly from the screen is shown in Figure 14c). Several gates can be set simultaneously. The data are then replayed and selected through successive and corresponding gates, all together or in a sequential order.

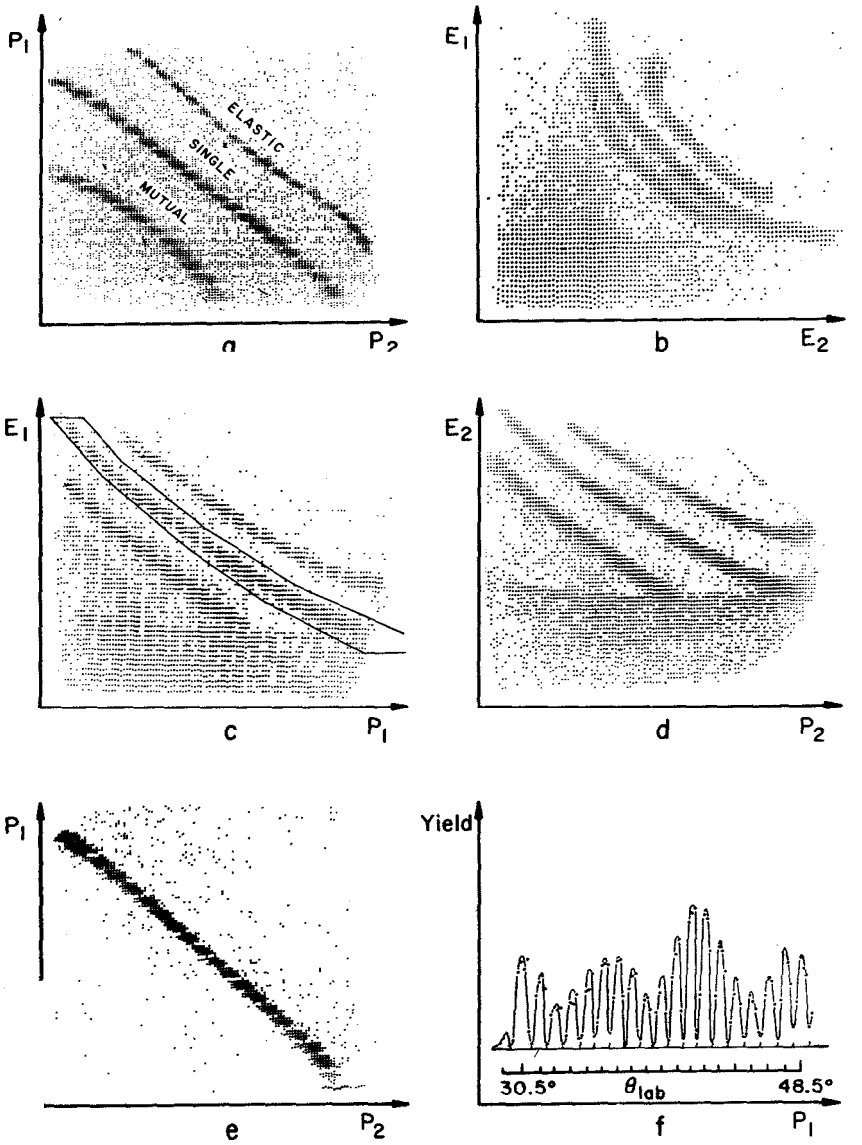

Figure 14 - Photographs taken directly from the data acquisition display. A more detailed discussion of the individual photographs is given in the text.

As an example we focus on the excitation of one of the C^{12} nuclei to its lowest 2^+ state. These events appear on a $P_1 - P_2$ plot as in Figure 14a) as the locus labelled SINGLE or as the gated region in Figure 14c). Once the gate is established it is readily moved by light pen control to an adjacent display region and reset for automatic background removal and in such a simple case as this the data are replayed through gates to yield the actual angular distribution data at 1" angular intervals shown in Figure 14f). The interval is here determined by a 1" raster grid over one of the detectors. Without such a grid of course very much finer angular resolution is available when

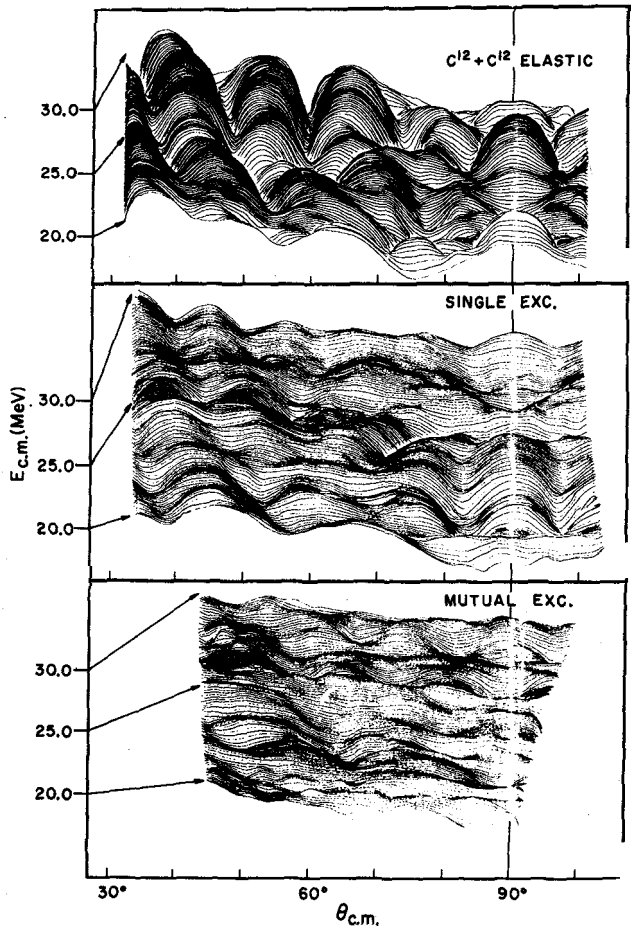

Figure 15 - Interpolated experimental data of the $C^{12} + C^{12}$ interaction showing the elastic, single and mutual excitation to the 2^+ state ($E_{x} = 4.43$ MeV).

needed. If desireú a subroutine can be called by pushbutton control to fit such data with any specified polynomial character and the coefficients displayed on the screen together with the data and the fit achieved. When required more extensive angular ranges are obtained by relocating the PSD to cover an adjacent kinematic field.

This $C^{12} + C^{12}$ interaction has been extensively studied. Our range of observation has been: $20 \leq E_{CM} \leq 30$ MeV measured in 250 keV intervals and $30 \leq \theta \leq 100°$. The enormous amount of data thus collected presents a very real problem in presentation. The most effective solution found has been to present the cross section data as an energy-angle surface as in Figure 5, with a three point interpolation in each direction, where required, in order to improve the visualization of the resulting surface. Figure 15 is such a presentation. This emphasizes the structure present at some sacrifice to a visualization of the exact magnitudes involveú. The

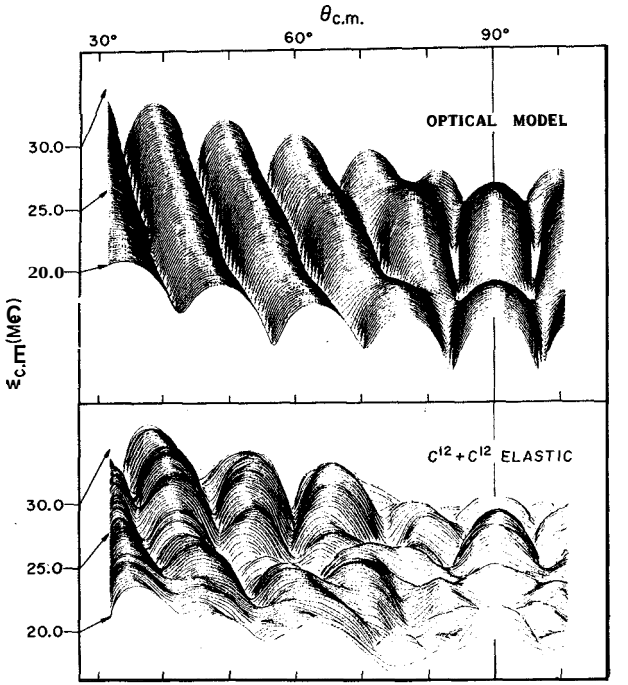

Figure 16 - Comparison of optical model calculations with the $C^{12} + C^{12}$ elastic scattering data This is to be compared with Figure 5 for the $O^{16} + O^{16}$ case; the much more complex structure of the C^{12} data is clearly apparent, although the optical model calculations successfully reproduce the gross features of these data

cross section is plotted on a logarithmic scale. At forward angles and low energies the single and mutual excitation are reduced in magnitude from the elastic by factors between five and ten. Going to more backward angles and higher energies the situation is reversed with the single and mutual excitation becoming predominant. All these results must be symmetric about $\theta_{CM} = 90°$. The elastic and single excitation provide, at high bombarding energies, a striking illustration of the Blair phase rule[26].

Figure 16 is a comparison of this experimental elastic scattering data with the optical model calculations based on Table I parameters. The relatively greater importance of the intermediate structure in the $C^{12} + C^{12}$ system is readily apparent in a comparison of Figures 5 and 16.

7. Neutron Transfer at Large Radius

Since, as is well known, the amplitude for transfer of a neutron between interacting nuclei is a direct measure of the overlap of the neutron wavefunctions relative to the initial and final cores it follows that at very large interaction radii the wavefunctions themselves have very small amplitude and in consequence the transfer amplitude becomes unmeasurably small. But just this behavior at large radius is of particular interest in many nuclear problems. In the formal sense, of course, the transfer amplitude can be considered as nothing more than a sum over the tails of a very large number of distant resonance states in the continuum.

Fortunately just this same experimental approach provides an approach to the measurement of this transfer amplitude. If we examine, for example, the $C^{12} + C^{13}$ elastic scattering system we must add coherently the elastic scattering amplitude A_s and that for neutron transfer, A_t, where $A_s \gg A_t$:

$$\frac{d\sigma}{d\Omega} \cong |\bar{A}_s + \bar{A}_t|^2 = A_s^2 + A_t^2 + 2\bar{A}_s \cdot \bar{A}_t \approx A_s^2 + 2\bar{A}_s \cdot \bar{A}_t .$$

It thus follows that in the interference term $A_s \cdot A_t$ the large elastic scattering amplitude acts to amplify the effect of the smaller transfer amplitude. This was first pointed out by Gobbi et *al.*[27]

Figure 17 shows a series of angular distributions for the $C^{12} + C^{13}$ elastic scattering system measured at center of mass energies in the range from 10.4 to 20.8 MeV.

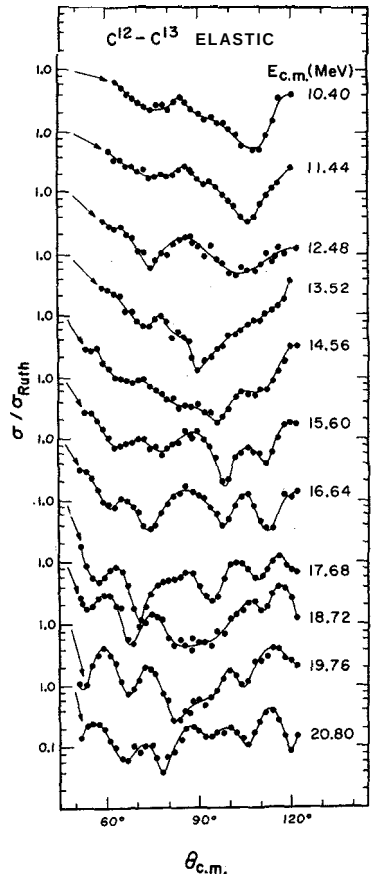

Figure 17 - Typical $C^{12} + C^{13}$ elastic scattering angular distributions.

Particularly striking, and in pronounced contrast to the situation for non-identical particles, as shown on the right side of Figure 6, for example, is the fact that particularly at the higher energies – but also at low – the individual peaks in the angular distributions do not move forward in angle with increasing energy. This is most strinkingly shown in Figure 18 where, on the right, we have modified our Table 1 elastic scattering potential appropriately for the $C^{12} + C^{13}$ case and have simply calculated the elastic angle-energy surface ignoring the possibility of transfer. On the left we have repeated this calculation but now have included a tranfer amplitude corresponding to the measure spectroscopic factor in the

$C^{12}(dp)C^{13}$ reaction and an assumed exponential wavefunction tail. We have used a formalism given by Von Oertzen[28]

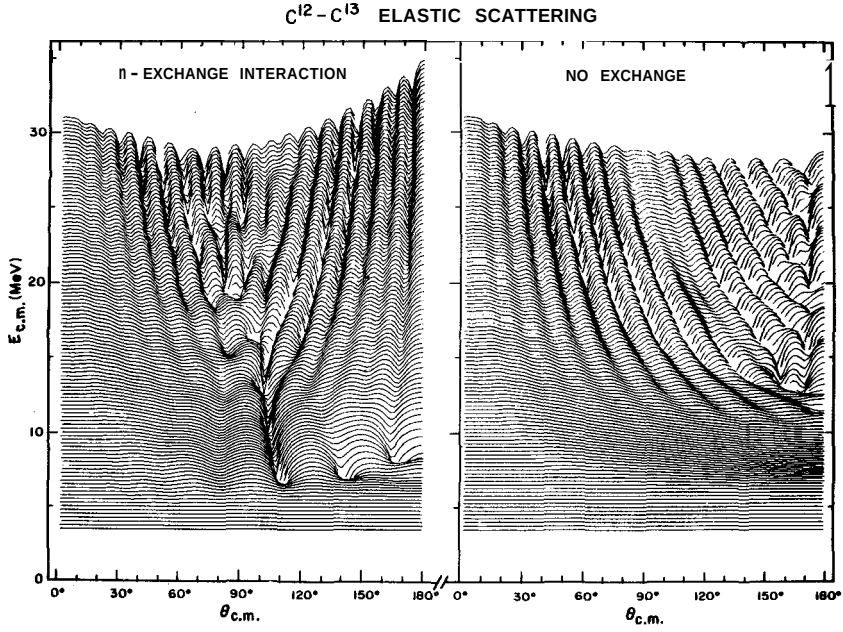

Figure 18 - Model prediction for the $C^{12} + C^{13}$ interaction. Plots show σ/σ_{Rutb} on a logarithmic scale.

The effects are striking; most obvious is the stabilization of the peaks in the angular distribution, at large angles, with changing energy. At a center of mass energy of some 7 MeV where striking structure already appears near 115" the pure elastic scattering cross sections remains smooth and indeed remains so until roughly twice this energy is reached.

We are currently completing a detailed analysis of an experimentally determined $C^{12} + C^{13}$ angle energy surface comparable to those of Figure 15 and hope soon to have new and detailed information on the neutron transfer amplitude; since the orbits of the C^{12} cores at least below the Coulomb barrier are classically determined we can vary the effective distance over which the neutron transfer occurs, hence the wavefunction overlaps, simply by varying the center of mass energy.

8. Cluster Structure in the Continuum

It has long been an open question in nuclear physics whether as energy was added to a nucleus its nucleons gradually heated up until one or more were evaporated, very much in analogy with a heated liquid droplet, or whether the increased energy might be effectively removed from the system through binding of relatively stable nuclear subunits, or clusters, which might have quite simple relative motions and low relative kinetic energies. It was early recognized that heavy ion reactions might provide a unique means for probing such configurations, if they existed, through direct transfer or pick up of the sub-units or clusters involved.

The earliest tandem accelerator measurements of Bromley *et al.*[22] provided evidence for such cluster configurations in Mg^{24} – in this case involving two C^{12} cluster – and led to the concept of quasimolecular nuclear configurations. Additional states of similar character have more recently been found by Patterson *et al.*[29] at slightly lower energies in Mg^{21} – well below the $C^{12} + C^{12}$ barrier. The existence of such configurations has been studied in a variety of theoretical models including that of Imanishi already mentioned and most recently those of Vogt[30] and Michaud and Vogt[31] who assume the alpha particle as the basic cluster sub-unit and view Mg^{24} as O^{16} plus two orbiting alpha particles.

The alpha particle or more generally "quartet"[2] structure is an attractive candidate for such behavior because of its intrinsic binding energy and the recognition that many of the light nuclei such as C^{12} and O^{16} show pronounced evidence for alpha particle substructure. This is further evidenced in the work of von Oertzen *et al.*[32] who find that the usual elastic scattering amplitudes for O^{16} on C^{12}, for example, must be combined coherently with an amplitude for alpha particle transfer in order to provide any adequate reproduction of the experimental elastic scattering data This is also suggested by the extensive $Ca^{40}(O^{16}, C^{12})Ti^{44}$ and similar alpha transfer studies of Faraggi *et al.*[33,34] at Saclay and of Friedman *et al.*[35] at Argonne and the initial successes of the Saclay theoretical group of Gillet *et al.*[36] in understanding these data on the basis of a quartet model.

Figure 19 shows the level diagram for Mg^{24}. The positions of the quasimolecular resonances[22] are indicated in Figure 19 at $\sim$ 20 MeV excitation in Mg^{24} and are now known[29] to extend down to $\sim$ 17 MeV excitation. Also indicated in Figure 19 are the positions of the 0^+ members of the lowest quartet configurations predicted by Arima et *al.*[37], where [x, *y*, *z*] denotes the number of clusters in the lp, 2s-ld and 2p-1*f* shells, respectively.

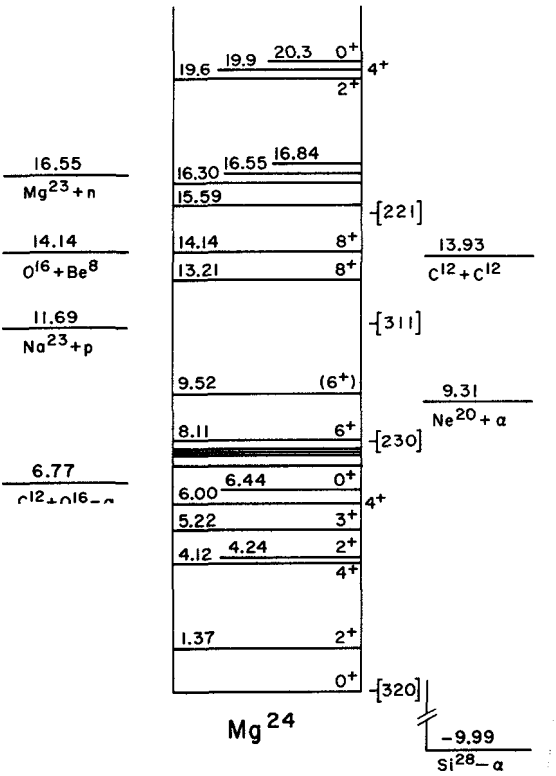

Figure 19 - Energy level diagram for Mg^{24} showing selected levels of interest to the present experiment, together with the threshold energies for the available decay channels. Predicted positions of quartet configurations are also shown.

In the region above the $C^{12} + C^{12}$ binding energy at $\sim$ 14 MeV it is well known that there is a high and rapidly increasing level density. Under these conditions it has been customary to assume that no individual states could be observed in any given reaction and spectra such as that of Figure 20 showing the $N^{14}(N^{14}, \alpha)Mg^{24}$ reaction data measured by Middleton et al.[38] at Pennsylvania were expected. Figure 21, obtained by a joint Yale-IBM group[39], shows a similar absence of any observable structure corresponding to highly excited states. A rather striking constrast occurs in the $Ne^{20}(Li^{6}, d)Mg^{24}$ reaction measured by Middleton et *al.*[40] and shown in Figure 22 Here a wealth of structure appears, presumably reflecting a much higher intrinsic selectivity in the reaction toward population of

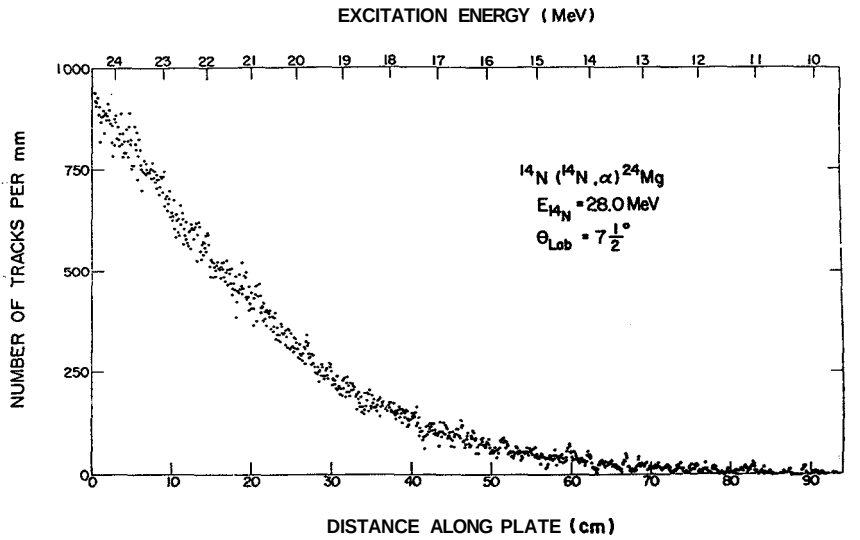

Figure 20 - Alpha particle spectmm from the $N^{14}(N^{14}, \alpha)Mg^{24}$ reaction as measured by Middleton *et al.*, at an incident N^{14} energy of 28.0 MeV.

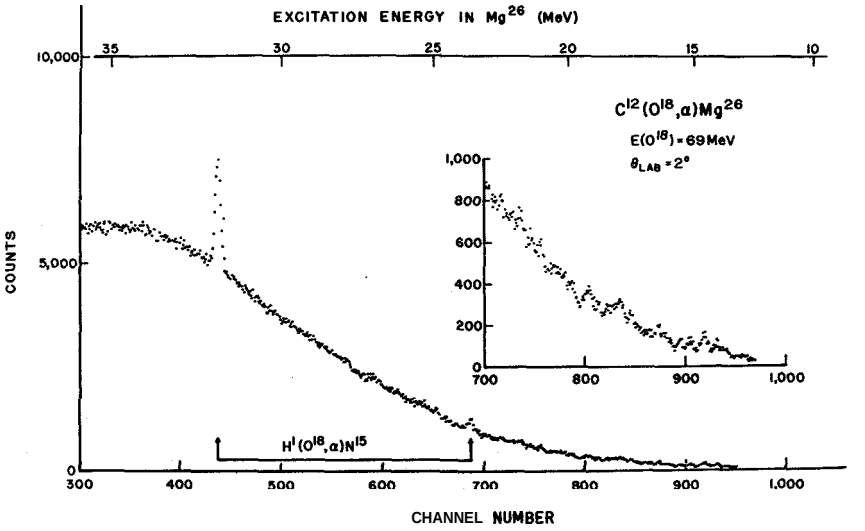

Figure 21 - Alpha particle spectmm observed in the $C^{12}(O^{18}, \alpha)Mg^{26}$ reaction. The insert shows the region of excitation energy in Mg^{26} from 13 to 23 MeV with the vertical scale expanded by a factor of 5.

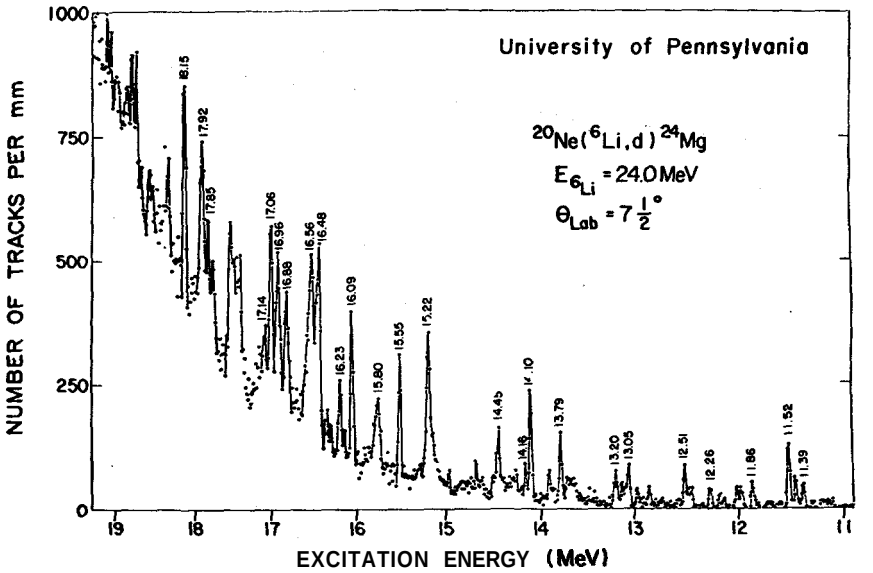

Figure 22 - Deuteron spectrum from the $Ne^{20}(Li^{6}, d)Mg^{24}$ reaction as measured by Middleton et al. at an incident Li^{6} energy of 24.0 MeV.

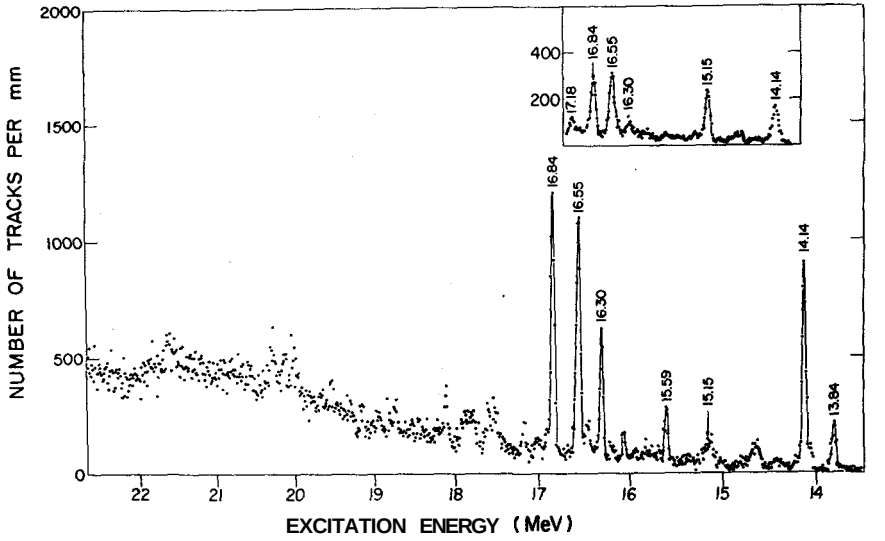

Figure 23 - Alpha particle spectra from the $O^{16}(C^{12}, \alpha)Mg^{24}$ reaction as measured by Middleton *et al.* at an incident C^{12} energy of *36.0* MeV. These data were obtained using the Pennsylvania magnetic spectrograph.

residual states having significant alpha particle reduced widths. Even more striking, however, as shown in Figure 23, was the result obtained by Middleton et *al.*[41] for the $O^{16}(C^{12},\alpha)Mg^{24}$ reaction. Figure 24 shows our own data, taken at a somewhat smaller angle but with a semiconductor particle detector, hence poorer intrinsic resolution. This was a reaction that had long been of interest to us in terms of possible search for lower $C^{12} + C^{12}$ quasimolecular states in Mg^{24}. Coulomb barrier effects preclude any direct study of possible $C^{12} + C^{12}$ configurations at lower energies closer to the 13.93 $C^{12} + C^{12}$ binding energy. Such states would, of course, be of particular interest in terms of their possible role in stellar carbon burning and some time ago we and a number of groups at other laboratories undertook a search of this region of excitation utilizing the $C^{12}(O^{16},\alpha)Mg^{24}$ reaction in the anticipation of observing a direct transfer of a C^{12} cluster from the O^{16} projectile. This mechanism would enable formation of a $C^{12} + C^{12}$ configuration much closer to threshold without direct interference from the Coulomb barrier. Middleton's first magnetic multigap spectrograph measurements, as shown in Figure 24, indicated that this reaction was very highly selective populating only a limited number of very sharp states ($\Gamma \leq 20$ MeV) in the 14-16 MeV range of excitation. (It should be emphasized again that the level density is known to be high in this region; over 40 states have been observed in the Na^{23} + p reaction between 12 and 13 MeV of excitation in Mg^{24}, for example.)

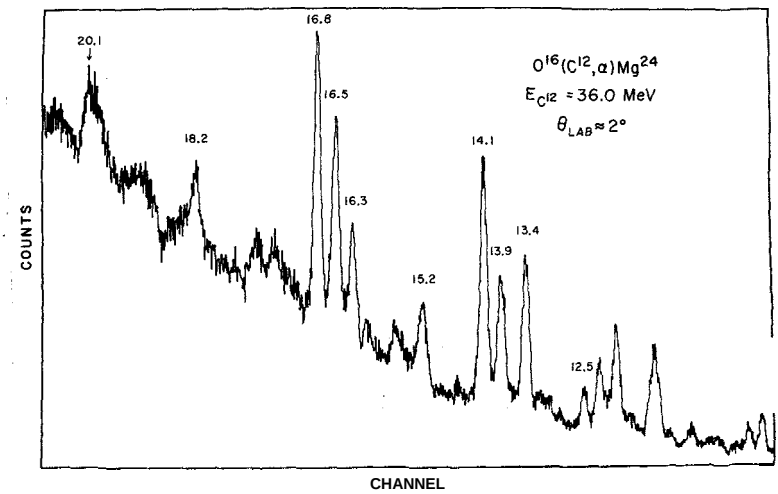

Figure 24 - Alpha particle spectrum from the $O^{16}(C^{12},\alpha)Mg^{24}$ reaction as measured at Yale at an incident C'' energy of 36.0 MeV. These data were obtained using a semiwnductor alpha particle detector.

The fact that these and subsequent measurements in several laboratories showed a pronounced excitation near 14 MeV, one near 15 MeV, and a triplet of states near 15 MeV suggested a vibrational sequence based possibly on a $C^{12} + C^{12}$ intrinsic structure. As a first approach to understanding these remarkably sharp states we undertook a series of angular correlation studies directed toward a determination of their spins and parities.

9. Angular Correlation Studies

The spin and parity J^{π} of a level in Mg^{24} can in principle be measured by observing the angular correlation of successive alpha particles in the two step reaction $C^{12}(O^{16}, \alpha_1)Mg^{24}(\alpha_2, Ne^{20})$. Fig. 25 shows the range of excitation in Mg^{24} over which this technique was applicable for the three separate center-of-mass energies which were used. If α_1 is detected at 0° and a, decays to Ne^{20} (g.s.), the $a, -\alpha_2$ correlation can be readily shown to have the simple form $\{P_J(\cos\theta)\}^2$; in practice the decay branch to Ne^{20} (g.s.) must be observed if a *unique* value of J is to be obtaineú, since mixed transitions can enter the formalism for final Ne^{20} states of non-zero spin, and these correlations have relative featureless structure.

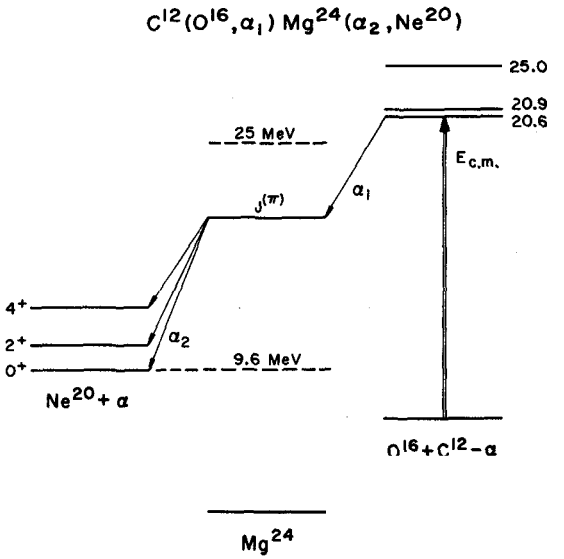

Figure 25 - A schematic level diagram showing the states involved in the angular correlation determinations of J^{π} assignments to states in Mg^{24} populated in the $O^{16}(C^{12}, \alpha)Mg^{24}$ reaction

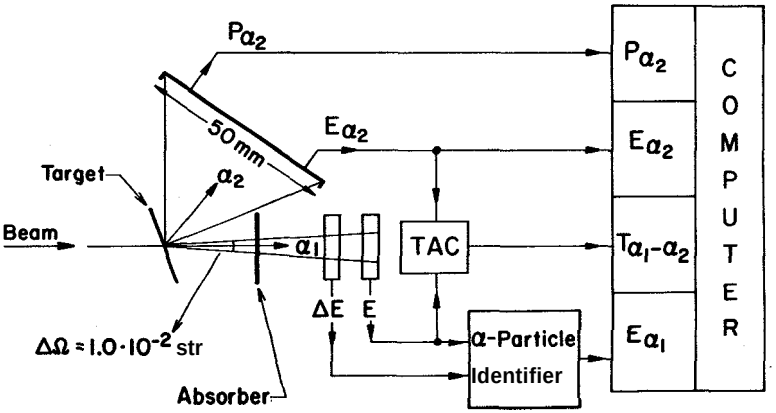

Figure 26 - A schematic diagram of the instrumentation used in the alpha particle double correlation studies.

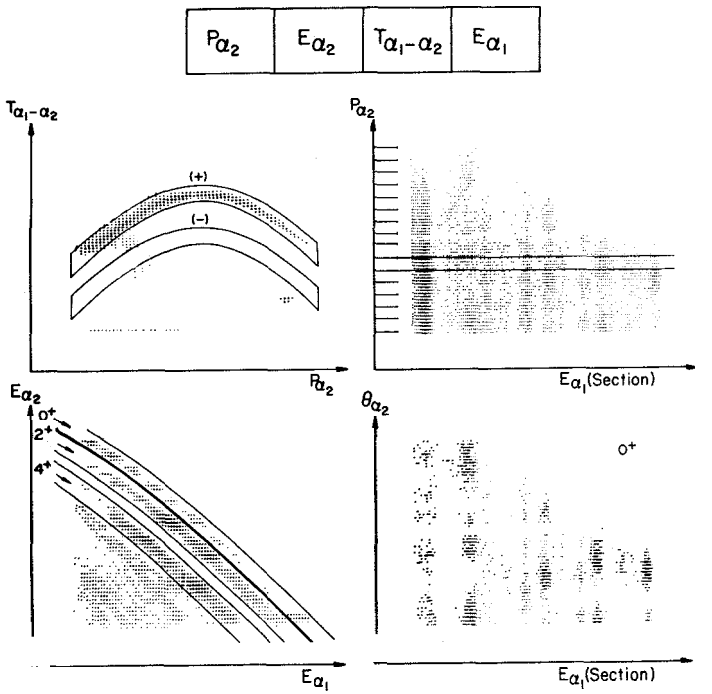

Figure 27 - Direct photographs from the data acquisition system display. The individual photographs are discussed in the text.

The experimental arrangement used is illustrated schematically in Fig. 26. Beams of 48.0, 48.8 and 58.3 MeV O^{16} ions impinged on a 20 μgm/cm carbon foil, the beam being stopped in a series of silver and nickel absorbers placed in front of a counter teleswpe. The 10 mm x 50 mm position sensitive detector subtended angles from 25° to 900 (lab). Digitized position, energy and time signals were stored in the laboratory's on line computer and written on magnetic tape. A multidimensional analysis using the wmputer display and light pen enabled the selection of the desired events; the various stages of this procedure are shown in Fig. 27 which shows direct photographs of the display. The solid curves indicate the two-dimensional

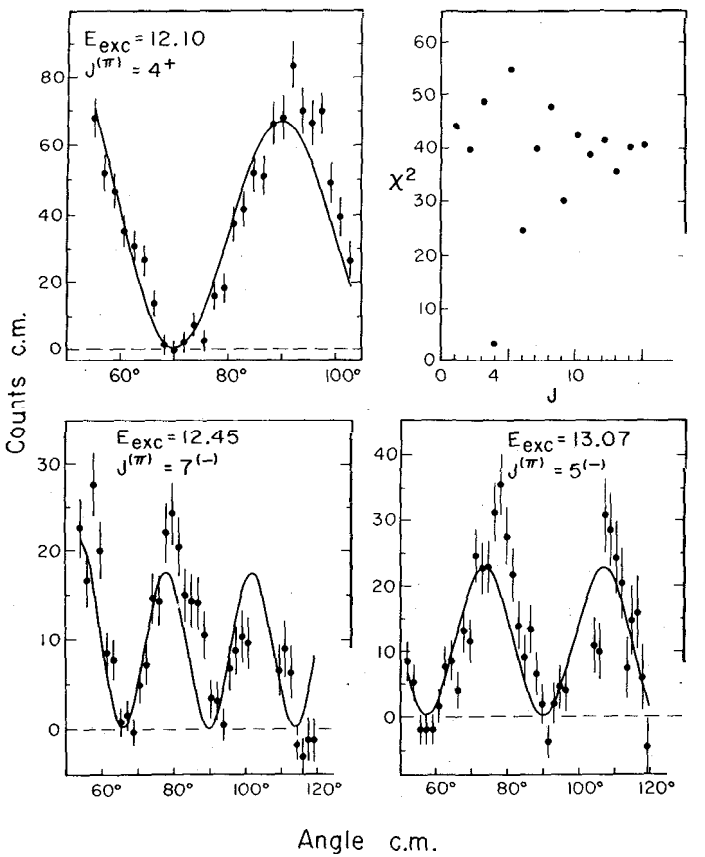

Figure 28 - Alpha particle angular wrrelations in the decay of selected states in Mg^{24}. The upper right figure shows the typical x^2 attained in the analyçis of these wrrelations.

regions or gates in which an event had to lie to be accepted. These ore simply drawn on the system's oscilloscope display with a light pen. True-plus-random, and random events were first selection in the $T_{\alpha_1-\alpha_2}-P_{\alpha_2}$ plane. The kinematic lines in the $E_{\alpha}-E_{\alpha}$ plane (for a fixed position, P_{α}) distinguished the decays to the different states of Ne^{20}. This process was repeated for all positions and resulted in the events shown in the $P_{\alpha}-T_{\alpha_1}$ plane, all of which correspond to decays to Ne^{20} (g.s.). Position has been converted to laboratory angle in the final section of Fig. 27. There, a pro-

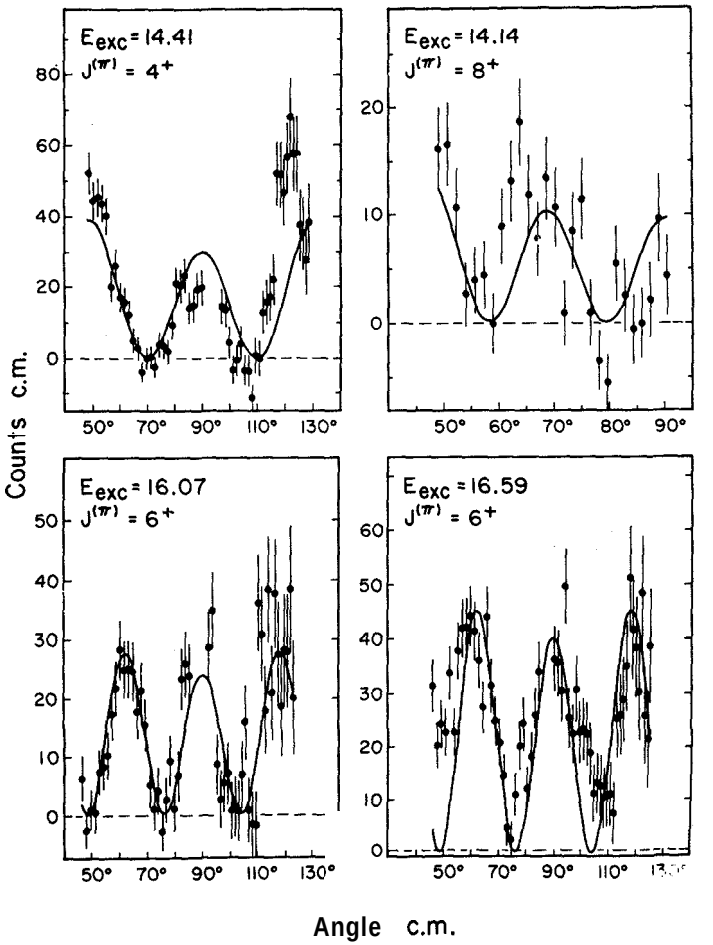

Figure 29 - Alpha particle angular correlations in the decay of selected states in Mg^{24}.

jection of all events into the E_{α} axis yields a spectrum which can be used for extraction of a branching ratio (when compared with similar spectra for the 2^+ and 4^+ states of Ne^{20}). If a particular region of E_{α} (corresponding to a definite state in Mg^{24}) is projected onto the θ_{α_2} axis, the desired correlation is obtained. Although some of the P_J^2 distributions are already visible in Fig. 27, Figs. 28 and 29 show more distinctly the correlations obtained for certain states after a constant background (in the laboratory system) was subtracted. Also shown in these figures are the least squares fits of $\{P_J(\cos\theta)\}^2$ to the data. Unique spin assignments for states other than these shown here were not possible because of insufficient intensity, relative to back ground, of the ground state decay. A plot χ^2 per degree of freedom as a function of J is given for least squares adjustments to the data for the 12.10 MeV state; note the sharp minimum at $J = 4$.

These measured high spins clearly precluded any interpretation in terms of a vibrational $C^{12} + C^{12}$ quasi-molecular configuration In order to obtain further insight into the structure of these states we undertook a more detailed study of the reaction mechanisms involved.

10. Reaction Mechanisms

The possible mechanisms for the reaction vary in a continuous manner from that of the statistical compound nucleus to that of the direct transfer of eight or twelve nucleons. Midway between these extremes lies the concept of intermediate structure in which the reaction proceeds through a broad state in the compound system whose lifetime is only somewhat longer than the typical collision time associated with a direct reaction. Governing all of the possible types of mechanisms will be the approximate selection rules imposed by the Coulomb and angular momentum barriers in the entrance and exit channels; in fact, these considerations by themselves go a long way towards explaining the fact that high spin states are preferentially populated in this particular reaction, where the exit channel cannot carry away the large angular momenta brought in by the heavy ions in the entrance channel.

Certain aspects of the information available on the $O^{16}(C^{12},\alpha)Mg^{24}$ reaction and on related reactions support different pictures for the reaction mechanism, and the possibility that the reaction contains contributions from several different mechanisms cannot be excluded. The formation of a statistical compound nucleus is suggested by the observation[42-45] of rapid changes in cross section with bombarding energy. The mechanism

for the population of the lowlying states in Mg^{24} has already been shown by Halbert et al. to be generally consistent with compound-nucleus formation [46,47]. Furthermore, states at high excitation energy in Al^{27}, presumably also of high spin, are selectively populated in the $C^{12}(O^{16}, p)Al^{27}$ reaction[48] at $E_{O^{16}} = 36$ and 60 MeV, and it is unlikely that such a reaction would proceed by a mechanism other than compound-nucleus formation.

In support of a direct mechanism for population of these states at high excitation energies, one can cite the smooth, generally forward peaked angular distributions presented in Ref. 41, and the fact that asymmetries about 90° center-of-mass angle in the angular distributions have been observed[49]. Furthermore, both the projectile and target nuclei themselves have a propensity for cluster-type structure which would enhance a direct transfer of a-clusters. The $C^{12}(N^{14}, d)Mg^{24}$ reaction[49] also selectively populates a number of states at high excitation in Mg^{24}, some of which may be identified (at least on the basis of measured energies) with those seen in the $C^{12}(O^{16}, \alpha)Mg^{24}$ and $O^{16}(C^{12}, \alpha)Mg^{24}$ reactions[41,49]. This is consistent with the transfer of a C^{12} or three a-particles occurring in these reactions. On the basis of such a direct-transfer model, one might expect that the $N^{14}(N^{14}, \alpha)Mg^{24}$ reaction would not selectively populate the aforementioned states, and this is indeed observed to be the case[3*].

However, the $N^{14}(N^{14}, \alpha)Mg^{24}$ results[38] may also be interpreted in terms of a compound-nucleus mechanism since the angular momentum matching conditions here are quite different than those of the $O^{16}(C^{12}, \alpha)Mg^{24}$ and $C^{12}(O^{16}, p)Al^{27}$ reactions. Table II lists the angular momentum conditions in the entrance and exit channels for a number of reactions for the excitation of a state at $\sim$ 17 MeV in the residual nucleus. (The channel radius is given by $1.44(A_1^{1/3} + A_2^{1/3})$fm). For the reactions such as $C^{12}(O^{16}, \alpha)Mg^{24}$, $C^{12}(O^{16}, p)Al^{27}$, and $C^{12}(N^{14}, d)Mg^{24}$ the population of states in the residual nucleus with high angular momentum should be greatly favor& by the large angular momentum mismatch between the entrance and exit channels, as represented by $\Delta(kR)$. The observation of the selective population of high spin states by these reactions is in agreement with these angular momentum considerations. In the case of the $N^{14}(N^{14}, \alpha)Mg^{24}$ reaction the angular momenta in the entrance and exit channels are very nearly matched at the N^{14} energies used in Ref. 38. This condition is much more favorable for the population of low-spin states than in the measurements where $\Delta(kR)$ is large. This can account, therefore, for the evaporation-like spectrum of α-particles[38], since the low-spin states are broader and have a higher density than the high-spin states. Thus the selective or

non-selective behavior of all four of these reactions can be understood in terms of angular momentum balance.

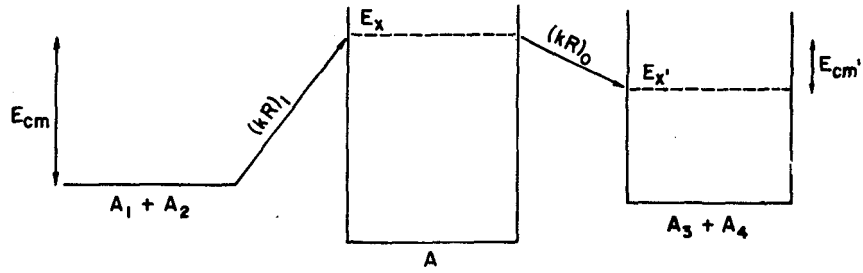

Reaction	E_{cm} (MeV)	$(kR)_i$	E_x (MeV)	E'_x ($E'_x = 17$ MeV)	$(kR)_0$	$\Delta(kR)$	Selective
$C^{12} + O^{16} \rightarrow Mg^{24} + He^4$	20.6	17.9	37.4	10.4	8.4	9.5	Yes
	25.7	20.0	42.5	15.5	10.2	9.8	Yes
$C^{12} + O^{16} \rightarrow Al^{27} + p$ [a]	25.7	20.0	42.5	13.9	4.6	15.4	Yes
$N^{14} + N^{14} \rightarrow Mg^{24} + He^4$ [b]	10.1	12.7	37.3	10.3	8.3	4.4	No
	14.0	15.0	41.2	14.2	9.8	5.2	No
$C^{12} + N^{14} \rightarrow Mg^{24} + d$ [c]	22.1	17.6	37.2	8.8	5.3	12.3	Yes
	25.4	18.9	40.5	12.1	6.2	12.7	Yes
$C^{12} + O^{18} \rightarrow Mg^{24} + He^6$ [d]	28.0	21.8	51.7	6.6	8.3	13.5	No
$C^{12} + O^{18} \rightarrow Mg^{26} + He^4$ [d]	28.0	21.8	51.7	24.0	13.0	8.8	See Fig. 2

Table II - a) Ref. 13, b) Ref. 15, c) Ref. 14, d) Ref. 16

The measurements[39] at Brookhaven on the $C^{12}(O^{18}, He^6)Mg^{24}$ and $C^{12}(O^{18}, \alpha)Mg^{26}$ reactions are not as unambiguous in their interpretation. The results presented in Fig. 23 for the $C^{12}(O^{18}, \alpha)Mg^{26}$ reaction indicate some selective population of states below $\sim$ 22 MeV in Mg^{26}, but these states are not very prominent over the evaporation-like background. Yet the angular momentum mismatch is only one unit lower than for the $C^{12}(O^{16}, \alpha)Mg^{24}$ reaction at 17 MeV excitation, and the mismatch increases for higher excitation energy, where no structure is observed at all. It might be argued that the small value of E'_{CM} for the $C^{12}(O^{18}, He^6)Mg^{24}$ reaction would inhibit its population of the high spin states near 17 MeV in Mg^{24}; however, the reaction should still selectively populate the high-spin states near 12 MeV in Mg^{24} for which $E'_{CM} \rightarrow 11.6$ MeV and $\Delta(kR) = = 10.8$. No such selective population was observed.

Another possibility for the $O^{16}(C^{12},\alpha)Mg^{24}$ reaction mechanism, in addition to the direct and compound pictures, is that of intermediate structure in the Si^{28} compound system. The existence of a-cluster or quartet structure at high excitation energy in Si^{28} was suggested by the calculations of Arima et *al.*[37]. This was previously noted in Ref, 37 as a possible explanation for the width of the structure observed in excitation functions measured[43] in the range E_{CM} = 19.7-21.3 MeV. Recently, Gastebois et al. have reported[45] excitation functions measured over the region E_{CM} = = 19.3-24.0 MeV and have noted a strong correlation in the cross sections for states in Mg^{24} at 15.15 MeV and at 16.55 MeV excitation. (The state at 16.55 MeV is actually an unresolved doublet[41].) They suggest that this may constitute evidence for quartet-type[37] intermediate structure in Si^{28}.

The present experiments have been undertaken in order to resolve some of the existing ambiguities in the interpretation of the mechanism of the $O^{16}(C^{12}$, a) Mg^{24} reaction. The most straightfonvard and thorough method for establishing the nature of a reaction mechanism consists of measuring complete angular distributions for each of many closely spaced bombarding energies, as has been done by Halbert et *al.*[46,47] for the states in Mg^{24} below 6 MeV. Such a measurement is a formidable task. Fortunately, a statistical compound nuclear mechanism requires that cross sections be symmetrical about 90° C.M., when averaged over an energy which is large compared to the fiuctuation width ($\sim$ 250 keV at E_{CM} −20 MeV). Thus, the existence of a direct or intermediate-structure component in the reaction mechanism can be detected by measuring excitation functions at two symmetric angles over an energy range large compareci to the fluctuation width.

Early in the measurements at Yale and at Pennsylvania it became apparent that the angular distributions of the α_1 groups populating states in certain cases were markedly anisotropic. Figure 30 compares measurements made at the same center-of-mass energy but with target and projectile roles reversed. The contrast between the behavior of the groups corresponding to states at 14.41 and at 14.14 MeV is striking. As illustrated in Fig. 31, if a direct mechanism were assumed, forward peaking of the α_1 distribution for an O^{16} beam would correspond preferentially to transfer of a C^{12} or of three alpha particles, whereas fonvard peaking of the a, distribution for a C^{12} beam would correspond preferentially to transfer of Be^8 or of two alpha particles.

We have, therefore, measured excitation functions in the range $E_{CM} \sim 18 \rightarrow$ $\rightarrow$ 21 MeV for an oxygen beam bombarding a natural carbon target and

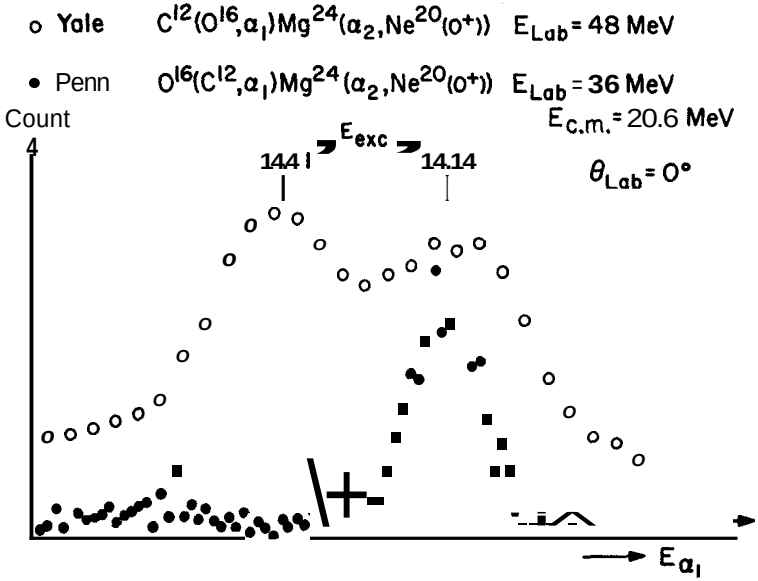

Figure 30 - Comparative 0° alpha particle spectra from the $C^{12}(O^{16}, \alpha)Mg^{24}$ and $O^{16}(C^{12}, \alpha)Mg^{24}$ reactions.

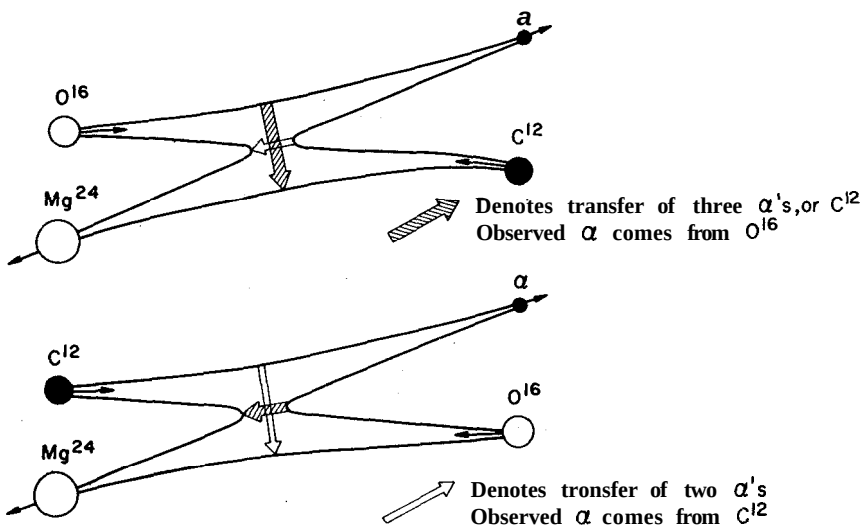

Figure 31 - Schematic representationof the $C^{12}(O^{16}, \alpha)Mg^{24}$ and $O^{16}(C^{12}, \alpha)Mg^{24}$ reactions on the assumption of a direct transfer mechanism.

for a carbon beam and silicon monoxide target. In each case, the a particles were detected at $\theta_{lab} \sim 2°$, which corresponds to center-of-mass angles of $\sim 3°$ and $\sim 177°$ respectively. The advantages of measuring at very forward angles in the laboratory system are twofold – cross sections are generally larger and a larger detector solid angle (6.2×10^{-3} sr.) may be used. The disadvantage with such an arrangement, however, is that an absorber is required in front of the detector to prevent the forward scattered heavy ions from reaching the detector. The α particle straggling in this absorber then places a lower limit on the resolution which can be attained. This limit for a ~ 13 mg/cm^2 Ni absorber is ~ 150 keV. This problem has been greatly reduced by the apparatus shown in Fig. 32. The absorber system shown here consists typically of 2 mg/cm^2 of Havar and ~ 2 mg/cm^2 of hydrogen. The straggling expected for this is ~ 100 keV, which represents a signiíicant improvement over the use of metallic absorbers. In addition the absorber thickness is easily varied to correspond to changes in beam energy.

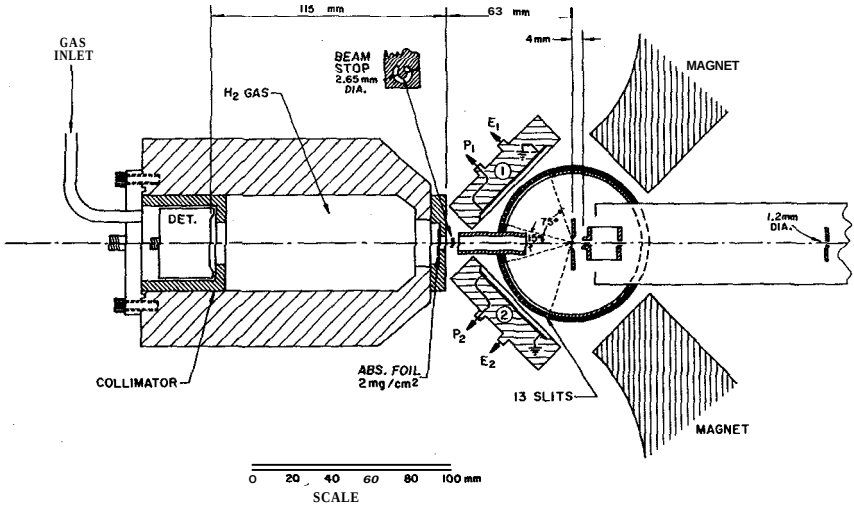

Figure 32 - Scale drawing of target-detector geometry used for the measurement of excitation functions for the $C^{12}(O^{16}$, a) and $O^{16}(C^{12}, \alpha)$ reactions. After passing through the target, the incident beam is stopped in the tantalum beam stop. (2.65 mm in diameter and 1.5 mm thick). The 2 mg/cm^2 Havar absorber foil and H, gas (typically at a pressure of 2 atmospheres) were used to prevent the forward scattered heavy ions from the target from reaching the $Si(SB)$ detector.

The results we obtained with this system are presented in Fig. 33 for $E_{C^{12}} = 35.63$ and $E_{O^{16}} = 47.60$ MeV which correspond to very nearly the same center of mass energy.

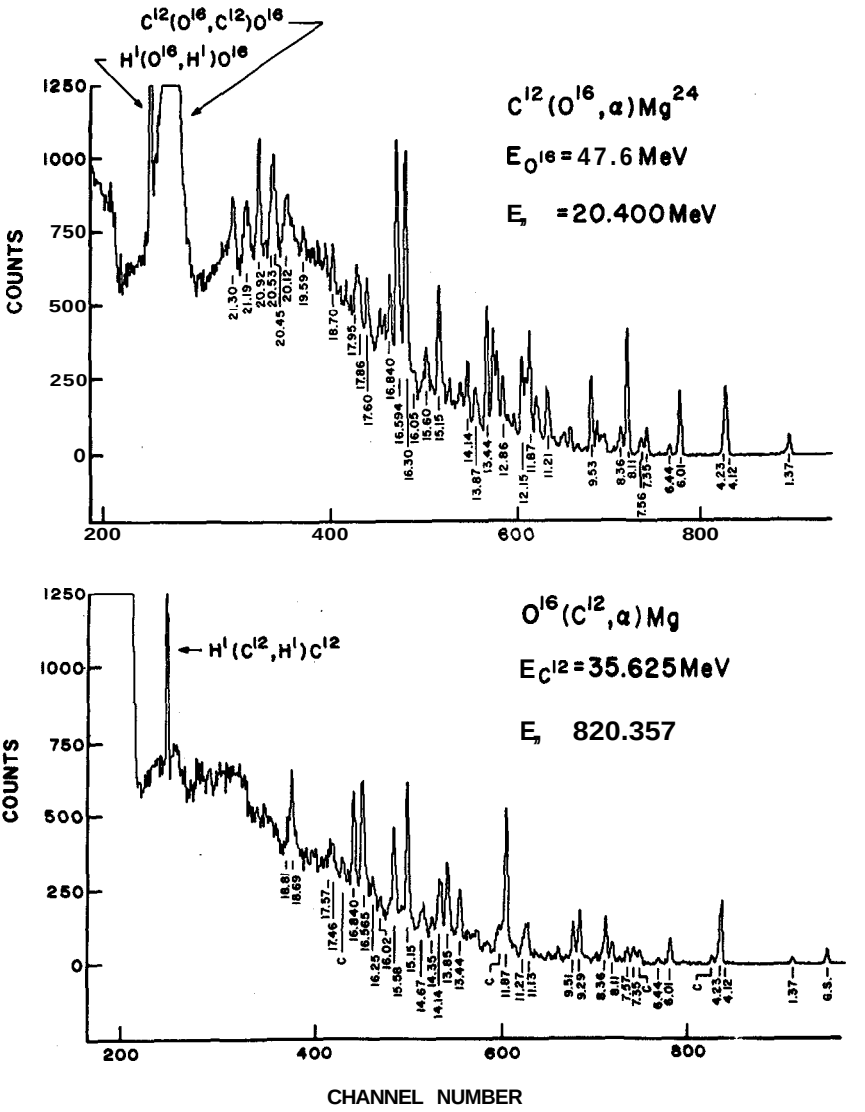

Figure 33 - Alpha particle spectra from the $C^{12}(O^{16}$, a) and $O^{16}(C^{12}$, a) reactions. Peaks are labelled by their excitation energies in Mg^{24}. The peaks labelled "C" in the $O^{16}(C^{12}, \alpha)Ne^{20}$ reaction on carbon contaminants.

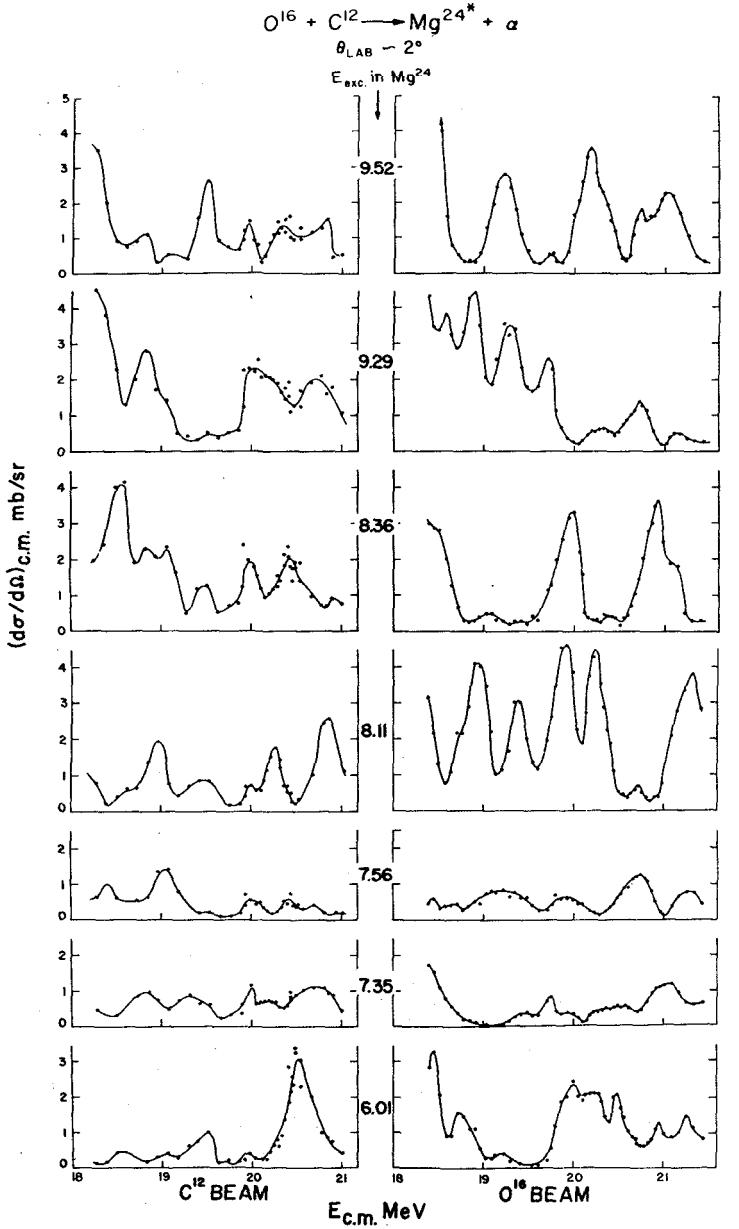

Figure 34 - Excitation functions measured at $\theta_{lab} \approx 2°$ for the $C^{12}(O^{16}, a)$ and $O^{16}(C^{12}, a)$ reactions populating states in Mg^{24} between 6.0 and 9.5 MeV in excitation. The uncertainty in the absolute cross section is ± 30%.

The various peaks in the spectra in Fig. 33 are labelled with their corresponding excitation energies in Mg^{24} and, for strongly populated states, have uncertainties of $\pm$ 25 keV in the region $E_x \leq 15$ MeV and $\pm$ 50 keV for the region ≥ 17 MeV. Weakly populated states have somewhat larger errors.

Peak position and areas were determined by simultaneously fitting up to six Gaussian functions on a linear background. Absolute cross sections were obtained by lowering the beam energy below the Coulomb barrier and normalizing to the Rutherford cross section. The individual measurements were normalized to the number of particles scattered at 45° by a film of gold of a few $\mu gm/cm^2$ thickness which had been evaporated onto the target.

Preliminary excitation functions have been extracted for many of the states appearing in the spectra of Fig. 33. In fourteen cases it was possible to follow groups which correspond, with reasonable confidence, to the same state in Mg^{24}. In other cases, the presence of contaminant peaks or unresolved doublets rendered this difficult. Fig. 34 presents excitation functions measured for low-lying states of Mg^{24}. These excitation functions are very similar to those observed for states below 6 MeV by Halbert et *al.*[46,47], and successfully analyzed in terms of a statistical compound nuclear mechanism. The cross sections for these states do not exhibit any apparent correlation in their respective dependencies on energy and angle, and, when averaged over energy, the cross sections are nearly symmetric, with maximum deviations from symmetry being approximately a factor of 2. A detailed analysis of the energy-averaged asymmetry and its statistical significance is in progress.

Excitation functions for states at higher excitation in Mg^{24} are presented in Figs. 35 and 36. Here again, the fluctuations of $\sim$ 250 keV width arising from statistioal compound-nucleus formation are present. However, of the cases measured with the C^{12} beam and plotted here all but one of the cross sections show a distinct correlation with a width of $\sim$ 1.5 MeV upon which the fluctuations are superimposed. This type of correlation (observed here for seven states) is inconsistent with the statistical model and constitutes direct evidence of the existence of a broad structure in the $O^{16}(C^{12},\alpha)Mg^{24}$ reaction. (Note that these states were not chosen on the basis of the existence of such a correlation but only on the technical consideration of being able to confidently extract peak areas from the observed spectra.)

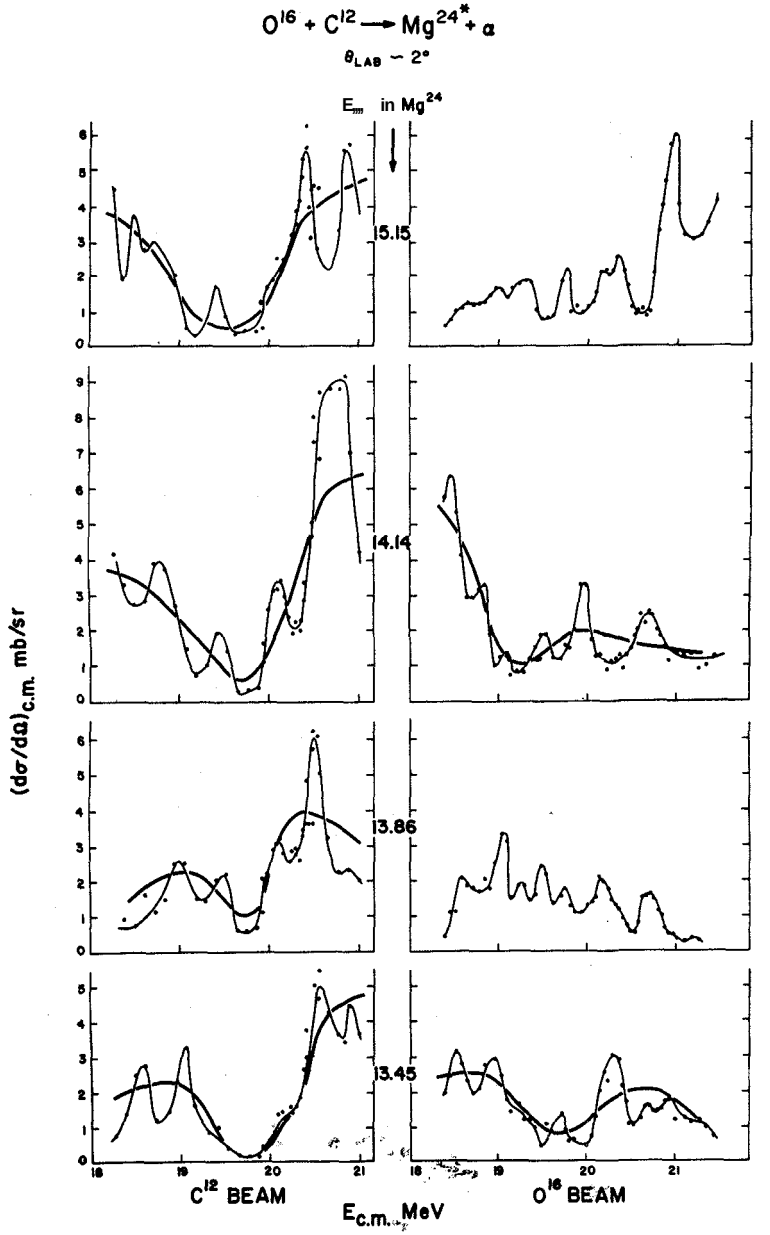

Figure 35 - Excitation functions measured at $\theta_{lab} \approx 2°$ for the $C^{12}(O^{16}, \alpha)$ and $O^{16}(C^{12}, \alpha)$ reactions populating states in Mg^{24} between 13.4 and 15.5 MeV in excitation. The uncertainty in the absolute cross sections is $\pm$ 30%.

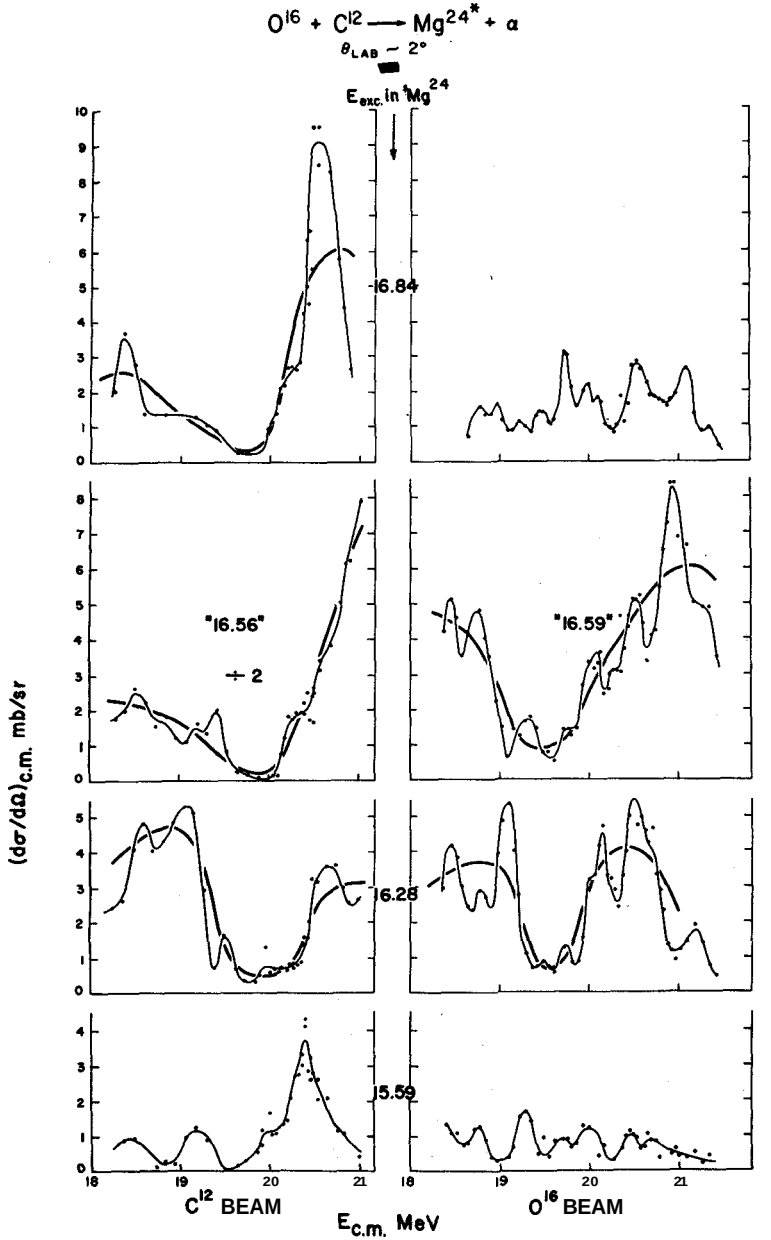

Figure 36 - Excitation functions measured at $0_{lab} \approx 2°$ for the $C^{12}(O^{16}, a)$ and $O^{16}(C^{12}, a)$ reactions populating states in Mg^{24} between 16.3 and 16.84 MeV in excitation. The uncertainty in the absolute cross section is $\pm$ 30%.

There are several other important features to be noted in Figs. 34-36. Although the states at 13.44 MeV and 16.28 MeV show roughly similar correlations for both beams (i.e. both angles), the correlations present for the states at 13.86 and 16.84 MeV, populated with the C^{12} beam, are clearly absent when these states are populated with O^{16} beam.[50] Thus, correlations of $\sim$ 1.5 MeV width are observed some of which exhibit approximate symmetry about 90° CM and some of which are clearly asymmetric. Furthermore, the state at 15.15 MeV (noted by the Saclay group[45]) appears to show the broad, correlated structure above $E_{CM} \sim 20$ MeV, but not below this energy. Finally, we note that the correlations, present for many states above 13 MeV in Figs. 35 and 36 are absent for those states shown in Fig. 34, i.e. for states below 10 MeV excitation.[51]

These features of the excitation functions and the broad structure exhibited by the $O^{16}(C^{12}, \alpha)Mg^{24}$ reaction may be understood to a large extent with the a-cluster model of Arima, Ginocchio and Gillet[37]. In this model, the broad structure would correspond to the formation of a-cluster states at $\sim$ 26-39 MeV excitation in Si^{28}, again relatively simple states very high in the continua. Such formation is greatly enhanced by the fact that both target and projectile are a-conjugate nuclei. The observed width of $\sim$ 1.5 MeV for the broad structure implies, furthermore, that one or more of the α-particles in Si^{28} at this excitation energy is loosely bound. The formation of cluster states in Si^{28} will therefore be enhanced for partial waves corresponding to grazing collisions while the somewhat lower partial waves will favor the formation of the statistical compound nucleus. Thus, the states in Mg^{24} which are strongly coupled to the Si^{28} system show a broad correlation with statistical fluctuations superimposed thereon. In the following discussion, we shall refer to the broad structure as an "*intermediate*" structure, reflecting its interpretation in terms of the formation of an intermediate state in the Si^{28} system.

The cluster states relevant to the intermediate structure, if preferentially induced by high partial waves, must have high angular momentum and therefore are not expected to correspond to the $J^\pi = 0^+$ "band head" energies in Ref. 37. For a given configuration of states of interest lie above the band head energy and may correspond to the recoupling of the α-particles of a particular structure to higher angular momentum, e.g. rotational cluster states.

The absence of intermediate structure in the low-lying states can also be accounted for by the quartet model. The low-lying states in Mg^{24}, if of a quartet nature, would be predominantely of the [320] configuration (see

Fig. 20). These states have a large overlap with the low-lying states of $Si^{28}[330]$, which are of the form $Mg^{24}[320] + a$. However, the cluster states populated at $\sim$ 38 MeV in Si^{28} (of the type [231], [312] and [222]) have little overlap with the low-lying states of Mg^{24} but can overlap with the higher-lping states of Mg^{24} (see Fig. 20).

The interpretation of the presence, for some states, and absence for others of broad structure at symmetric center-of-mass angles is somewhat ambiguous. We note that the $\sim$ 1.5 MeV width of the intermediate structure implies a lifetime of $\sim 4 \times 10^{-22}$ sec. for the compound system. This is of the order of the nuclear traversal time for the emitted a-particle, so that asymmetry in the angular distributions for the broad intermediate structure might be expected for some states. This characteristic lifetime is, however, also comparable to the collision time of the O^{16} and C^{12} ions in the entrance channel, which suggests that a direct reaction mechanism may also explain some of the results for particular states. With regard to the uniqueness of the interpretation in terms of a-cluster intermediate structure, we note that a width of $\sim$ 1.5 MeV approaches the width of the gross struo ture observed in heavy ion elastic scattering studies (Ref. 53). This suggests that the observed structure might be associated with a sharply defined (in energy space) absorption of partial waves corresponding to a grazing collision. Such an effect in the entrance channel would naturally imply a structure in the elastic scattering and other channels of width similar to that observed in the Mg^{24} and a-channel and with a definite phase relationship. Measurements on the elastic and inelastic scattering cross sections are in progress and should provide an answer to these questions. It is also possible that the above mentioned mechanism is intimately related to that of a broad intermediate structure of α-clusters in the Si^{28} compound system.

Generally, however, the results presented in Figs. 33-35 may be understood with the quartet model[37] and may therefore be interpreted as evidence for the existence of a-cluster structure for highly excited continuum states in Mg^{24} and in Si^{28} and for the presence of intermediate structure in the $O^{16}(C^{12},\alpha)Mg^{24}$ reaction.

Assuming an interpretation in terms of the a-cluster model, several speculative comments may be made concerning both the reaction mechanism and this structure. First, the structure observed for the 14.14 state, which has been assigned[19] as the 8^+ member of the $K^\pi = 2^+$ band in Mg^{24}, would suggest that this band contains, at high excitation, a cluster-like component in its wave function (most likely [230]). Second, we note that the

absence of intermediate structure for the low-lying states also suggests that the a-cluster states in Si^{28} are not strongly coupled with the states of the statistical compound nucleus, but remain rather pure in spite of their broad width and high excitation energy. An interesting test of this suggestion would be to measure excitation functions for $C^{12}(O^{16}, p)Al^{27}$ reactions. In this case, the intermediate structure, present in the entrance channel, should not be coupled to the exit channel as it can be in the case of $C^{12}(O^{16}, \alpha)Mg^{24}$, and one would not expect to see any broad structure in the excitation function. The lack of structure in the a-particle spectra for the $N^{14}(N^{14}, \alpha)Mg^{24}$ reaction[38] may be explained both on the basis of angular momentum matching and statistical compound nucleus formation and on the basis of the expected absence of intermediate structure, since neither projectile nor target is a-conjugate. The $C^{12}(O^{18}, \alpha)Mg^{26}$ reaction[39] shows some indication (Fig. 22) of a selective population of states in the region below 22 MeV, but the absence of strongly populated states, such as are present in the $C^{12}(O^{16}, \alpha)Mg^{24}$ reaction (Fig. 33), is striking. Apparently, the addition of the two neutrons to O^{16} in the entrance channel and to Mg^{24} in the exit channel greatly reduces the propensity of these nuclei to form a-clusters.

Although the present investigation of the importance of a-cluster phenomena in the structures of Mg^{24} and Si^{28} and in the $O^{16}(C^{12}, \alpha)Mg^{24}$ reaction mechanism has yielded new information on the nature of the α-cluster states in the continuum, there remain, however, a number of interesting questions to be answered.

11. The Structure of Continuum States in Mg^{24}

We have focussed thus far on the importance of a-cluster phenomena in the structure of high-lying states in Mg^{24}. The question of the existence of even heavier clusters in Mg^{24} is the logical consequence of both the the experimental results just described and the quartet model. Do quartets themselves couple to configurations which resemble a Be^8 or C^{12} nucleus? The experiments of Bromley et *al.*[22] and Patterson et *al.*[29] indicate that $C^{12} + C^{12}$ molecular configurations are important. Michaud and Vogt[31] interpret these results not in terms of C^{12} "molecules" but rather in terms of three a-particles coupled to a C^{12} core. In either case, the measurements of Ref. 22 show that the resonances in the $C^{12} + C^{12}$ reaction at and below the Coulomb barrier are of low spin (see Fig. 20). However, in the present experiments it is known that the $C^{12}(O^{16}, \alpha)Mg^{24}$ reaction selectively populates high-spin states. An experiment was therefore designed specifi-

cally to search for heavy-cluster configurations of high spin in Mg^{24} by direct observation of the decay of Mg^{24} into heavy cluster components. The various decay modes and their thresholds are shown in Fig. 20.

From our earlier correlation work on the decay of the sharp states in Mg^{24} above 11 MeV of excitation it was already clear that alpha particle emission was by far the strongest decay mode. In order to detect heavier nuclei in the presence of such a large background of α-particles, a second position sensitive detector was added to the system shown in Fig. 26 in order to measure the positions and energies of all three particles present in the final states of the reaction. The resulting over-determination of the properties of the final state is an indispensable tool in the analysis of the data.

A schematic diagram of the apparatus and data handling system (using our IBM 360/44 computer) is given in Fig. 37. The position sensitive detectors were collimated to ▬ 7 mm x 50 mm and covered laboratory angles from 15" to 75°. The detection system at 0° was as described earlier. The experiment was performed at $E_{O^{16}} = 58.3$ MeV with a $\sim 20\ \mu gm/cm^2$ carbon target. The seven linear pulses indicated in Fig. 37 were digitized for each triple coincidence and stored on magnetic tape as well as in the computer memory. Using the absolute position and energy calibrations for each of the three detectors, the digitized pulses were converted, by software, directly to units of MeV and laboratory angle.

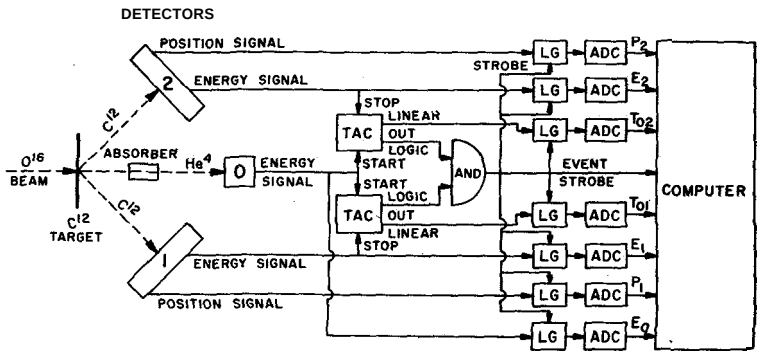

Figure 37 - Schematic diagram of the experimental arrangement used for the triple-correlation measurements.

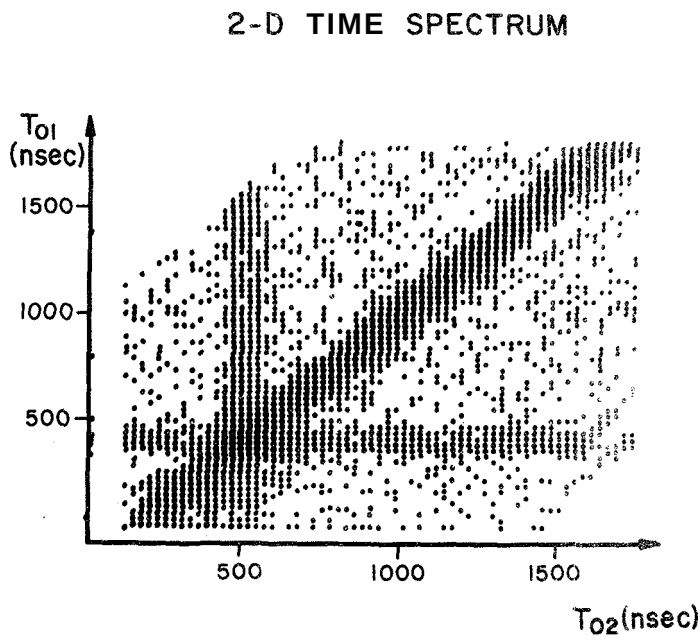

Figure 38 - Two-dimensional time spectrum obtained in ihe triple-correlation experiment. Real triple coincidences occur in the region near ($T_{01} = 400$ nsec, $T_{02} = 600$ nsec). The treatment of the various random coincidence contributions is discussed in the text.

The analysis of over two million triple-coincidence events proceeded in the following order. Each event was either passed or rejected by a series of one and two-dimensional gates which, cumulatively, enabled the determination of the species, excitation energy, and angular correlation of the reaction products. A two-dimensional time gate was first applied to sort the events according to their mutual relarionship in rime. Fig 38 presents a two-dimensional time spectrum with T_{01} plotted against T_{02}. The three types of random events which can occur in a triple coincidence experiment are clearly indicated. The diagonal line corresponds, for example, to events in which a true coincidence takes place in detectors 1 and 2 (see Fig. 37) and an a-particle arrives at a random time in the 0° detector. The intensity of this line arises from the high kinematic coincidence rate produced by heavy ion elastic and inelastic scattering into detectors 1 and 2. The vertical and horizontal lines arise from events in which a real coincidence occurs between detectors 0 and 1, and 0 and 2, with a random particle in the remaining detector. Triple coincidence events are located

at the intersection of these three lines. A rectangular gate ~ 100 ns wide was set around this region, and gates of identical size were placed along each of the three well defined random event lines, and also on the region which corresponds to a random event in all three detectors. Events passing through these gates were then appropriately flagged. A proper random subtraction for a triple coincidence experiment requires such a procedure, which is greatly facilitated by the use of event-by-event recording.

The detection of one of the three particles in the exit channel at 0° requires that the momenta of the other two particles transverse to the beam direction be equal and opposite. This requirement yields the relation

$$M_1/M_2 = E_2 \sin^2 \theta_2 / E_1 \sin^2 \theta_1 .$$

Since each of the quantities on the right-hand side of this equatión is measured directly, a "mass ratio" spectrum, as shown in Fig. 39, is easily obtained. This constitutes an effective determination of the individual particle species

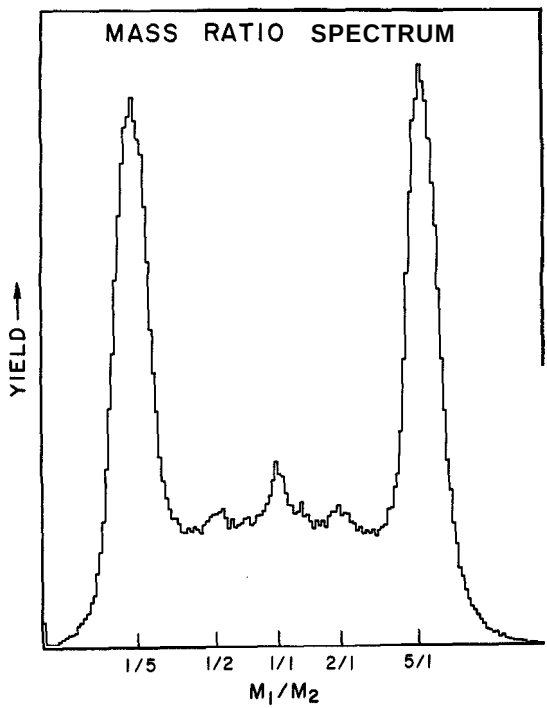

Figure 39 - Plot of mass-ratio spectrum of the decay products of states in Mg^{24}. The peaks at 1/5 and 5/1 correspond to decay to $Ne^{20} + \alpha$; the peaks at 1/2 and 2/1 correspond to decay into $O^{16} + Be^{8}$; and the peak at 1/1 to fission into $C^{12} + C^{12}$.

since the sum of the masses must equal 28 and the absorber renders the 0" detector sensitive only to light particles. The mass ratio spectrum exhibits symmetry about unity since the position sensitive detectors are symmetric about the beam axis. The background in this spectrum arises mainly from real triple coincidences corresponding to four-body break up. The large peaks at mass-ratio values of 1/5 and 5 correspond to a, + a + Ne^{20} and the peak at unity corresponds to a, + C^{12} + C^{12}. The peaks at 1/2 and 2 imply the observation of a, + Be^{8} + O^{16} in the exit channel. This is consistent with the geometry of the detection system and the typical angular opening of the cone of a-particles ($\sim 5°$, half-angle) defined by the inflight decay of the Be^{8} nucleus. A rough calculation indicates that the detection efficiency for both a-particles from the Be^{8} is well over 50%.

A one-dimensional gate was then set on each of the peaks in Fig. 39. Events in these gates were subjected to further scrutiny to eliminate the four-body background present in the mass plot. The known energies, positions, and masses of the particles in the 0' detector and in one of the position sensitive detectors were used to calculate the energy and position which the remaining particle must have in the other position-sensitivedetector. If the remaining particle was observed to have the correct position and energy (within some preset limits) the event was accepted.

The next step in the analysis was to determine the excitation energies of the now-identified out-going particles. The quantity $E_{O^{16}}$ + Q = E_0 + + E, + E, was determined based on the measured energies and positions of the two lightest particles and calculated energy of the heavy particle. Fig. 40 presents "Q-value" spectra for each of three gates set on the mass-ratio spectrum. The arrows denote the predicted positions of the peaks based on the absolute energy calibration of the three detectors.

The properties of the three-body final state were thus completely specified; it remains only to present the sorted events in a form designed to reveal the physical process under investigation. For our purposes, this form is a plot of the triple coincidence yield versus the excitation energy in Mg^{24}, this quantity being defined by the energy of the "first" a-particle, a,, observed at 0°. Figs. 41-44 present the triple coincidence yields for four outgoing channels as a function of the energy of the α-particle observed at 0". These figures display events which have passed through the gates set on the spectra in Figs. 38 (time), 39 (mass ratio) and 40 (Q-value). Real and random events were subjected to identical processing, the random events being subtracted only after all gates were applied. The cut-off at low a-particle energies, determined by the thickness of the absorber at 0", does not affect

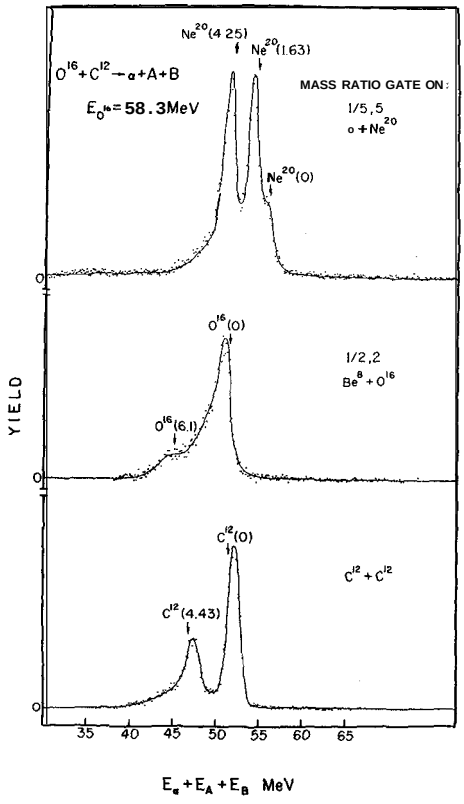

Figure 40 - Spectra for each of the 3 decay channels, plotted as a function of the total kinetic energy in the 3 body final state. Peaks are identified corresponding to the residual nuclei in their ground states and in various excited states.

the shape of the spectrum beyond íhe lowest two channels shown. The random to real-plus-random ratio was of the order of or less than a few percent in regions where the spectra contain more than $\sim$ 20 counts per channel. Finally, tests of interna1 consistency were made throughout the course of the analysis. No evidence for improper sorting of the events was found. An important externa1 check on the analysis is provided by the requirement that the angular distributions for break up of Mg^{24} into $C^{12} + C^{12}$ and with $C^{12} + C^{12}$ (4.4) be symmetric about 90"C.M. angle in the Mg^{24} system. The measured angular distribution exhibited this symmetry.

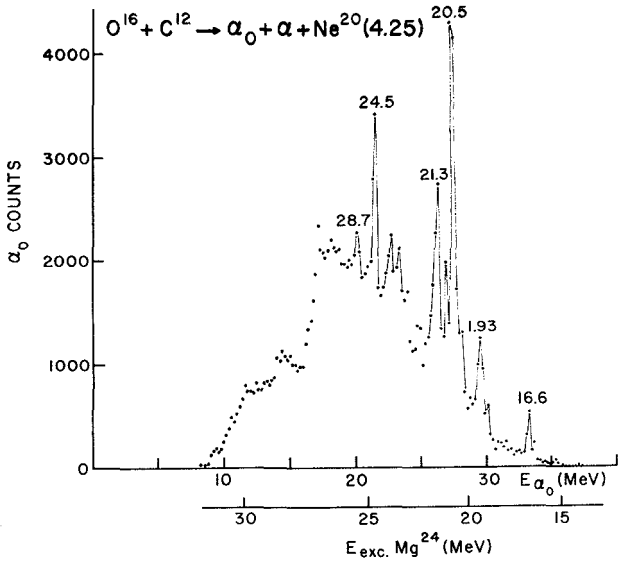

Figure 41 - Triple-coincidence yield as a function of E_{α_0} gatedby the peak in Fig. 12 corresponding to a final state comprised of $\alpha_0 + \alpha + Ne^{20*}$ (4.25).

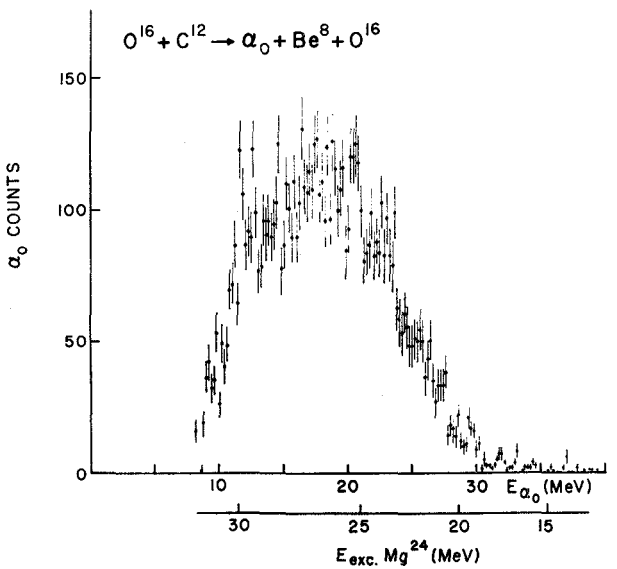

Figure 42 - Triple-coincidence yield as a function of E_{α_0} gated by the total $Be^8 + O^{16}$ spectrum in Fig. 12.

The sharp groups in Fig. 41 correspond to events in which the intermediate state of the $O^{16} + C^{12} \rightarrow \alpha_0 + a + Ne^{20}(4^+)$ reaction proceeded through definite states in Mg^{24}. The smoothly varying background underneath these sharp groups can arise from low spin states with large widths or from narrow states, each of which is populated with a small cross section, but which are very dense. Contributions to the background may also arise from the detection of the second α-particle (i.e. from the decay of Mg^{24}) a: 0° and the first α-particle in one of the position sensitive detectors.

Another mechanism, which can contribute to the yield in Fig. 41 but which does not involve the formation of Mg^{24}, is the break-up of the C^{12} nucleus into three a-particles, one of which attaches to the O^{16} projectile to form Ne^{20} (4.25). Thus, it is possible to demonstrate the formation of a state in Mg^{24} only if *a* distinct peak is observed in the E, spectrum.

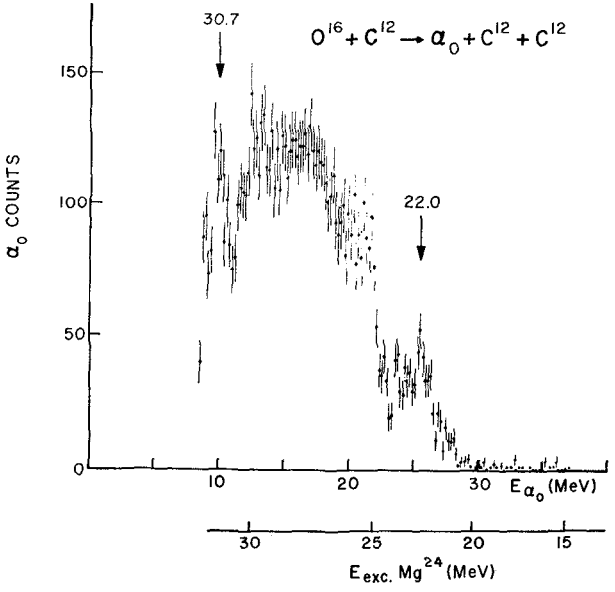

Figure 43 - Triple-coincidence yield as a function of E, gated by the ground-state peak in the $C^{12} + C^{12}$ spectrum in Fig. 12.

The spectra shown in Figs. 42-44 each exhibit a smoothly varying background similar in shape and in magnitude. In these cases, the reaction can proceed either by a break-up of the O^{16} projectile (Figs. **43,** 44) or

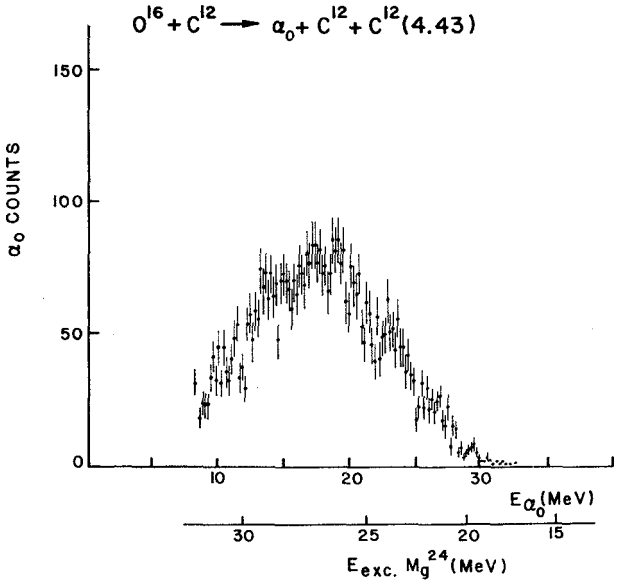

Figure 44 - Triple-coincidence **yield as a function of E,** gated **by the peak** in **Fig. 12 corresponding to a 3 body** final **state** comprised **of a,** $+ C^{12} + C^{12*}(4.43)$.

a break-up of the C^{12} target nucleus (Fig. 42), all of which processes are expected to yield a smoothly varying spectrum of a-particles. Indeed, the fact that the "backgrounds" in Fig. 43 ($\alpha_0 + C^{12} + C^{12}$) and in Fig. 44 (a, $+ C^{12} + C^{12}(4.4)$) are comparable argues in favor of a break-up mechanism; if the reaction proceeded through states in Mg^{24}, the much lower penetrability for the $C^{12}(4.4)$ channel would preclude the onset of this process until $\sim$ 25 MeV excitation in Mg^{24}. We have made optical-model calculations of transmission coefficients (Fig. 45) for the break-up of Mg^{24} into various clusters, and find that both the shapes and sizes of the gross background in Figs. 43 and 44 are inconsistent with the formation and decay of states in Mg^{24}. Analysis of the data in terms of a break-up mechanism is being undertaken to check the above arguments in more detail.

Having discussed the general shape of these four spectra, we note now the definite peaks in the a, $+ C^{12} + C^{12}$ spectrum (Fig. 43) at excitation energies of 22.0 and 20.7 MeV in Mg^{24}. It is unlikely that such sharp structure can arise from the direct break-up of the target or the projectile.[54] Were this not the case, the spectra of Figs. 42 and 44 should also show

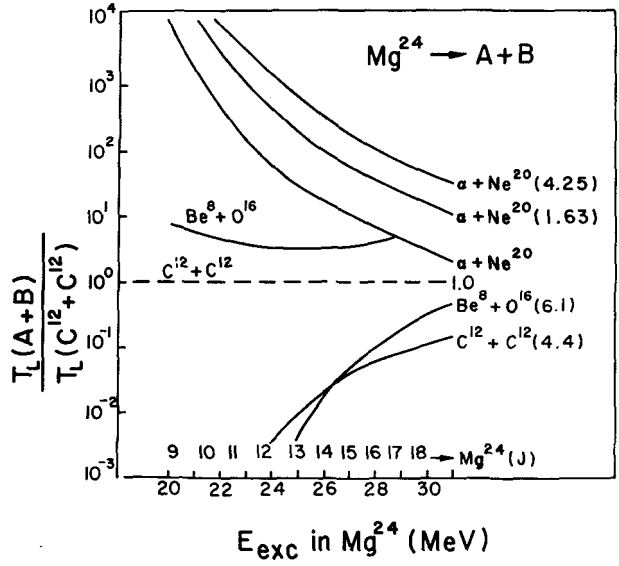

Figure 45 - Transmission coefficients for the various open channels for the decay of Mg^{24} have been calculated with an optical model code, and are plotted here, normalized to the $C^{12} + C^{12}$ transmission coefficient. For a given excitation energy in Mg^{24}, the orbital angular momentum, L, in the exit channel was determined by the l-value for which $T_l(\alpha_0) \approx 1/2$. For the particles in the ground state, L = J = 18-l, and this value is also given in Fig. 17, labelled as $Mg^{24}(J)$. This represents an approximate lower limit on the spin of states in Mg^{24*} which can be excited in the $C^{12}(O^{16}, \alpha)Mg^{24}$ reaction at $E_{O^{16}} = 58$ MeV. In cases where one of the nuclei in the exit channel has non-zero spin, this amount of angular momentum was subtracted from the orbital angular momentum to be carried away. Although these calculations are not very precise, they do give an order-of-magnitude guide to the selection rules imposed by the Coulomb and centrifugal barriers.

such structure. We cite these peaks, therefore, as evidence for states at 22.0 and 20.7 MeV in Mg^{24} which have C^{12}, C^{12} "molecular" configurations. The measured widths of these states[S5], respectively, are $\sim$ 380 keV and 230 keV, which is significantly larger than the width contributed by the resolution of the 0° detection system. These total widths are comparable to the Wigner limit for the reduced width $\sim$ 300 keV.

Angular distributions for the decay of these states are presently being analyzed and may allow limits to be placed on their spins. The state at 30.7 MeV is likely to have a high spin, e.g. in the region 12-18 units, as the α-particle leading to the formation of this state can carry away little

angular momentum. Similar arguments would place a lower limit of ~ 6-8 on the spin of the 22.0 MeV states. The measured widths of the states in terms of the Wigner limit, however, imply upper limits of ~ 4-6 and 10-12 for the states at 22.0 and 30.7 MeV, respectively. These arguments are crude and, of course, quite sensitive to the choice of channel radius. Nevertheless, the above considerations favor the interpretation of the states observed here as rather pure $C^{12} + C^{12}$ configurations rather than as configurations of three alpha particles outside a C^{12} core. Were this latter configuration present, the decay of the state by α emission would be much more strongly favored than C^{12} emission.

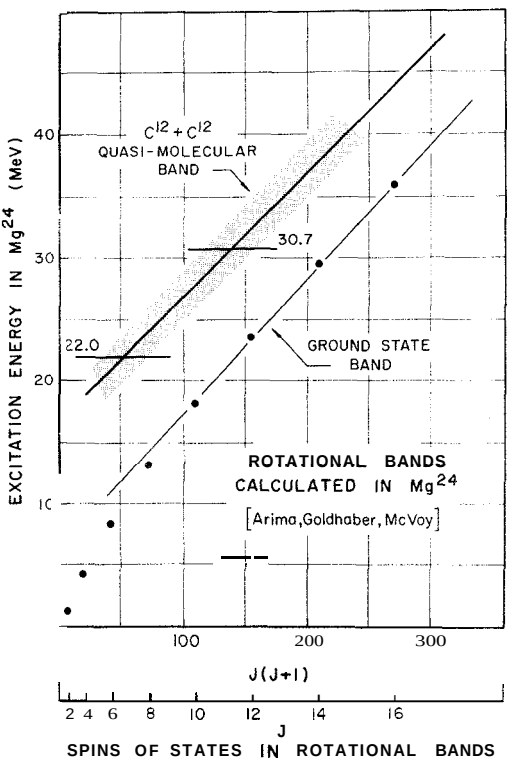

Figure 46 - Predicted quasi-molecular rotational band characteristics in Mg^{24}. The shaded area is the model estimate of the full width at half maximum of the predicted quasi-molecular band members. The horizontal heavy lines mark the excitation energies at which the $C^{12} + C^{12}$ decaying states, discussed in the text, have been located.

It is amusing, but very probably coincidental, to note that in a recent paper Arima *et al.*[56] consider the question of possible quasi-molecular rotational bands at very high excitation in Mg^{24}. Their argument is based on McVoy's recent Regge-type analysis of shape resonances, our potential parameters and use of the variable moment of inertia model to predict the probable location of the quasi-molecular band, given the observed properties of the ground state band. Fig. 46 reproduces their results for Mg^{24} with the excitation energies of our two $C^{12} + C^{12}$ states superposed; it is interesting to note that these intersect the predicted $C^{12} + C^{12}$ quasi-molecular trajectory at spins of about 6 and 12, respectively, which are the values common to the two estimates given above for each of our states. In the absence of any evidence, as yet, for other possible members of such a rotational band, this must be considered as coincidental. These authors have also made a rough estimate of the expected width of the states in the quasi-molecular band. This is indicated by the shaded area in the figure which extends to the calculated half maximum points. Clearly the experimental widths of the two states which we have observed are very much smaller than this estimate. Nonetheless we are now searching more carefully for other possible members!

The measurements[22,29] on the $C^{12}(C^{12}, C^{12})$ and $C^{12}(C^{12}, \alpha)$ reactions, which have located molecular resonances at excitation energies between 17 and 20.3 MeV excitation in Mg^{24}, preferentially populate states of low spin. This is shown by the measured spins[22] and by penetrability arguments, since the resonances occur at and below the Coulomb barrier. Thus the state seen at 30.7 in the present work by virtue of its inferred high spin, is probably not the same type of configuration as was observed at $\sim$ 20 MeV excitation[22]. The state at 22 MeV, depending on whether its spin is $\sim$ 6 or $\sim$ 10, may or may not be associated with the resonances observed in Ref. 22. The width of this state is $\sim$ 3 times larger than the molecular states at $\sim$ 20 MeV.

Although the analysis of these data is still in progress and the results should be regarded as preliminary, it appears that we have observed the production and decay of $C^{12} + C^{12}$ molecular configurations in Mg^{24} via the $C^{12}(O^{16}, \alpha)Mg^{24}(C^{12})C^{12}$ reaction.

12. Conclusions

Using heavy ion beams and on line computer based data acquisition instrumentation we have examined several types of new continuum nuclear structure. Via the elastic scattering of identical bosons we have studied

existing resonances of effective single particle character and double resonances wherein these are coupled, via interim inelastic excitation of either, or both, target and projectile, to quasi-bound lower lying resonances. We have used elastic scattering as a probe to amplify very weak transfer amplitudes in a special study of a rather classical direct reaction. Finally we have carried out a detailed study of very sharp high spin states in Mg^{24}. We have found evidence for the importance of quartet or alpha particle structure high in the continuum of both Mg^{24} and Si^{28} and have demonstrated that certain other continuum states at high excitation have measurable width for decay into $C^{12} + C^{12}$ and possibly also $Be^{8} + O^{16}$. We have only, as yet, a glimpse of the new configurations and new physics which await further exploration using high quality heavy ion beams characteristic of the large tandem accelerators and modern detection and data handling instrumentation. We welcome the new São Paulo Laboratory and the first of the Herb Pelletron accelerators into the tandem fraternity.

I am much indebted to my colleagues, both past and present, in the Wright Laboratory who have been very much involved in this work; they include Rolf Siemmsen, Martin Sachs, Adriano Gobbi, Peter Parker and Robert Stokstad. Without my students during the same period, James Maher, Richard Wieland, Wilfred Reilly, Daniel Shapira and Lowry Chua, little of this would have been accomplished. Finally, it is a pleasure to thank Edith Fehr, Charles Gingell and Kenzo Sato for vital assistance with both instrumentation and accelerator. Hana Novak for draftsmanship beyond the call of duty, and Mary Anne Thomson and Harriet Comen for, as always, producing finished papers from manuscript which even I can scarcely read.

References and Notes

1. W. Scheid, W. Greiner and R. Lemmer, Phys. Rev. Lett. 25, 176 (1970)
2. D. A. Bromley, J. A. Kuehner and E. Almqvist, Phys. Rev. **123,** 878 (1961).
3. R. W. Shaw, R. Vandenbosch and M. K. Mehta, Phys. Rev. Lett. 25,457 (1970).
4. R. H. Siemssen, H. T. Fortune, R. Malmin, A. Richter, J. W. Tippie and P. P. Singh, Phys. Rev. Lett. 25, 536 (1970).
5. J. V. Maher, M. W. Sachs, R. H. Siemssen, A. Weidinger and D. A. Bromley, Phys. Rev. **188,** 1665 (1969); J. V. Maher, Doctoral Dissertation, Yale University (1969) unpublished.
6. L. A. Jacobson, Phys. Rev. **188,** 1509 (1969).
7. W. Reilly, R. Wieland, A. Gobbi, M. W. Sachs and D. A. Bromley, ***Proceedings of*** the ***International Conference on Nuclear Reactions Induced by Heavy Ions, Heidelberg,*** 1969, edited by R. Bock and W. R. Hering (North-Holland Publishing Company, Amsterdam--London; American Elsevier Publishing Company, Inc., New York) p. 93.
8. W. Reilly, R. Wieland, A. Gobbi, M. W. Sachs, J. V. Maher, D. Mingay, R. H. Siemssen and D. A. Bromley, ***Ibid.,*** p. 95.

9. G. C. Morrison. H. T. Fortune and R. H. Siemssen, *Ibid,* p. 72.
10. D. A. Bromley, *Ibid.,* p. 27.
11. W. Scheid, R. Ligensa and W. Greiner, Phys. Rev. Lett. 21, 1479 (1968).
12. L. Rickertsen, B. Block, J. W. Clark and F. B. Malik, Phys. Rev. Lett. 22, 951 (1969).
13. R. A. Chatwin, J. S. Eck, D. Robson and A. Richter, Phys. Rev. Cl, 795 (1970).
14. J. S. Blair, ***Proceedings of the International Conference on Nuclear Reactions Induced by Heavv Ions, Heidelberg,*** 1969, edited by R. Bock and W. R. Hering (North-Holland Publishing Company, Inc., Amsterdam-London; American Elsevier Publishing Company, Inc., New York) p. 1.
15. P. H. Barker, A. Huber, H. Knoth, U. Matter, A. Gobbi and P. Marmier, Nucl. Phys. **A155,** 401 (1970).
16. P. J. A. Buttle and L. J. B. Goldfarb, ***Proceedings of the International Conference on Nuclear Reactions Induced by Heavy Ions, Heidelberg,*** 1969, edited by R. Bock and W. R. Hering (North-Holland Publishing Company, Inc., Amsterdam-London; American Elsevier Publishing Company, Inc., New York) p. 197.
17. H. A. Bethe in ***Facets of Physics,*** edited by ***D.*** A. Bromley and V. W. Hughes, Academic Press, New York, 1970.
18. R. J. Ascuitto and N. K. Glendenning, Phys. Rev. **181,** 1396 (1969).
19. R. H. Bassel, G. R. Satchler and R. M. Drisko, Nucl. Phys **89**, 419 (1966).
20. G. H. Rawitscher, private communication.
21. B. Imanishi, Nucl. Phys. **A125,** 33 (1969).
22. D. A. Bromley, J. A. Kuehner and E. Almqvist, Phys. Rev. Lett. 4,365 (1960).
23. H. L. Gelemter, J. Bimbaum, M. Mikelsons, J. D. Russell, F. Cochrane, D. Groff, J. F. Schofield and D. A. Bromley, Nucl. Instr. and Meth **54**, 77 (1967).
24. J. Bimbaum and M. W. Sachs, Physics Today, July (1968).
25. A. Gobbi, M. W. Sachs, R. Wieland, W. Reilly and D. A. Bromley, ***Proceedings of the International Conference on Nuclear Reactions Induced by Heavy Ions, Heidelberg,*** 1969, edited by R. Bock and W. R Hering (North-Holland Publishing Company, Inc., Amsterdam--London; American Elsevier Publishing Company, Inc., New York) p. 178.
26. J. S. Blair, in: ***Lectures in Theoretical Physics,*** 1965, Vol. VIIIC, eds. P. D. Kunz, D. A. Lind and W. E. Brittin (University of Colorado Press, Boulder, 1966) p. 343.
27. A. Gobbi, U. Matter, J. L. Perrenoud and P. Marmier, Nucl. Phys. **A112** 537 (1968).
28. W. Von Oertzen, Nucl. Phys **A148**, 529 (1970).
29. J. R. Patterson, H. Winkler and C. S. Zaidins, Ap. J. **157,** 367 (1969).
30. E. W. Vogt, ***Proceedings of the International Conference on Nuclear States,*** ed. by ***M.*** Harvey et al., University of Montreal Press (1969).
31. G. J. Michaud and E. W. Vogt, Phys. Lett. **30B**, 85 (1969); and preprint (1971).
32. W. Von Oertzen, H. H. Gutbrod, M. Müller, U. Voos and R. Bock, Phys. Lett. **26B**, 291 (1968); W. Von Oertzen, Nucl. Phys. **A148,** 529 (1970).
33. H. Faraggi, A. Jaffrin, M. C. Lemaire, M. C. Mermaz, J. C. Faivre, J. Gastebois, B. G. Harvey, J. M. Loiseaux and A. Papineau in the A. ***deShalit Memorial Volume,*** Annals of Phys., New York (1971).
34. J. C. Faivre, H. Faraggi, J. Gastebois, M. C. Lemaire, J. M. Loiseaux, M. C. Mermaz, A. Papineau, Phys. Lett. 24, 1188 (1970).
35. A. M. Friedman, H. T. Fortune, G. C. Morrison, R. H. Siemssen, ***Proceedings of the International Conference in Nuclear Reactions Induced by Heavy Zons,*** edited by R. Bock and W. Hering, North Holland Publishing Company, Amsterdam (1969).
36. V. Gillet, ***Proceedings of the International Conference on Quartet Structure,*** Saclay (1971) to be published.
37. A. Arima, V. Gillet and J. Ginocchio, Phys. Rev. Lett. **25,** 1043 (1970).
38. R. Middleton, J. D. Garret and H. T. Fortune, B.A.P.S. 16, 37 (1971).

39. M. J. LeVine, P. D. Parker and R. G. Stokstad (private communication).
40. R. Middleton *et al.*, (privatc communication) 1971.
41. R. Middleton, J. D. Garret and H. T. Fortune, Phys. Rev. Lett. **24,** 1436 (1970).
42. R. G. Stokstad, A. Gobbi, P. R. Maurenzig and R. Wieland, B.A.P.S. 15, 1677 (1970).
43. A. Gobbi, R. Stokstad, P. R. Maurenzig, D. Shapira, P. D. Parker and D. A. Bromley, *International* ***Conference on Heavy Ion Physics,*** Dubna, Feb. 1971.
44. L. R. Greenwood, T. H. Braid, K. Katori, R. H. Siemssen and J. C. Stoltzfus, B.A.P.S. 16, 645 (1971).
45. J. Gastebois, R. Ballini, P. Charles, B. Fernandez and J. Fouan, unpublished preprint.
46. M. L. Halbert, F. E. Durham and A. Van der Woude, Phys. Rev. 162,899 (1967).
47. M. L. Halbert, F. E. Durham, C. D. Moak and A. Zucker, Phys. Rev. 162, 919 (1967).
48. E. R. Cosrnan, E. Grosse, A. Graue and C. H. Britt, B.A.P.S. 16, 644 (1971).
49. A. Gobbi, P. R. Maurenzig, L. Chua, R. Hadsell, P. D. Parker, M. W. Sachs, D. Shapira, R. Stokstad, R. Wieland and D. A. Bromley, Phys. Rev. Lett. ***26,*** 396 (1971).
50. The excitation functions labelled "16.59" and "16.56" were extracted from groups which are known [41, 49, 52] to correspond to a doublet. Both members of the doublet are present at each angle with the 16.59 MeV state populated predominately by the O^{16} bearn and the 16.56 (16.54 in ref. 41) MeV state more intensely populated by the C^{12} beam, at $E_{,,,} = 20.5$ MeV. Our experimental resolution ($\sim$ 80 keV FWHM excitation in Mg^{24}) is insufficient to unfold the two cornponents and thus the excitation functions must be regarded as the sum of the two components. The correlation of the summed components and the large magnitude of the cross section ($\frac{da}{d\Omega_{CM}} \sim$ 16 mb/sr) at $E_{CM} = 21$ MeV for the carbon beam, however, are quite striking.
51. There are a great number of states present in the region of 17-22 MeV excitation. Analysis of this region and other regions is still in progress and includes a search for states which may exhibit an energy-averaged asymmetry with respect to 90" CM.
52. D. P. Balamuth, J. E. Holden, J. W. Noe and R. W. Zurmuhle, Phys. Rev. Lett. 26, 1271 (1971).
53. A. Gobbi, R. Wieland, W. Reilly, L. Chua, D. Shapira M. W. Sachs, R. Ascuitto and D. A. Bromley, "The Determination of Interaction Potentials for Heavy Ions". ***Sixth*** *International* ***Conference on Heavy Ion Physics,*** Dubna, USSR (1971).
54. Very recent measurements in this laboratory have shown that such structure can indeed arise from final state interactions between an alpha particle and a carbon nucleus involving specific states in O^{16} having large alpha particle width. It has been possible to show in fact that the peaks which appear in Figure 43 are primarily the result of such final state interactions although we cannot exclude the possibility of direct $C^{12} + C^{12}$ break up. These more recent measurements will be published in the near future.
55. It is possible, of course, that each of the observed peaks corresponds to a group of more narrow, unresolved states. In this case, the measured widths are only upper limits.
56. A. Arima, G. S. Goldhaber and K. W. McVoy, Phys Rev. Lett (in press) and pnvate communication (1971).